JGR Atmospheres

RESEARCH ARTICLE
10.1029/2019JD030509

Nuclear Winter Responses to Nuclear War Between the United States and Russia in the Whole Atmosphere Community Climate Model Version 4 and the Goddard Institute for Space Studies ModelE

Joshua Coupe[1], **Charles G. Bardeen**[2,3], **Alan Robock**[1], **and Owen B. Toon**[3,4]

[1]Department of Environmental Sciences, Rutgers University, New Brunswick, NJ, USA, [2]Atmospheric Chemistry Observations and Modeling Laboratory, National Center for Atmospheric Research, Boulder, CO, USA, [3]Laboratory for Atmospheric and Space Physics, University of Colorado Boulder, Boulder, CO, USA, [4]Department of Atmospheric and Ocean Sciences, University of Colorado Boulder, Boulder, CO, USA

Key Points:
- The climate response to a nuclear war between the U.S. and Russia is simulated in the WACCM4 climate model as a 150-Tg black carbon injection into the upper atmosphere and compared to an older experiment with GISS ModelE
- A true nuclear winter occurs in both models as black carbon aerosols block sunlight and cause global average surface temperatures to plummet by more than 8 K
- Fractal particle growth in WACCM4 reduces aerosol lifetime, but climate impacts are not diminished

Supporting Information:
- Supporting Information S1

Correspondence to:
J. Coupe,
josh.coupe@rutgers.edu

Citation:
Coupe, J., Bardeen, C. G., Robock, A., & Toon, O. B. (2019). Nuclear winter responses to nuclear war between the United States and Russia in the Whole Atmosphere Community Climate Model Version 4 and the Goddard Institute for Space Studies ModelE. *Journal of Geophysical Research: Atmospheres*, *124*, 8522–8543. https://doi.org/10.1029/2019JD030509

Received 20 FEB 2019
Accepted 16 JUL 2019
Accepted article online 23 JUL 2019
Published online 8 AUG 2019

Abstract Current nuclear arsenals used in a war between the United States and Russia could inject 150 Tg of soot from fires ignited by nuclear explosions into the upper troposphere and lower stratosphere. We simulate the climate response using the Community Earth System Model-Whole Atmosphere Community Climate Model version 4 (WACCM4), run at 2° horizontal resolution with 66 layers from the surface to 140 km, with full stratospheric chemistry and with aerosols from the Community Aerosol and Radiation Model for Atmospheres allowing for particle growth. We compare the results to an older simulation conducted in 2007 with the Goddard Institute for Space Studies ModelE run at 4° × 5° horizontal resolution with 23 levels up to 80 km and constant specified aerosol properties and ozone. These are the only two comprehensive climate model simulations of this scenario. Despite having different features and capabilities, both models produce similar results. Nuclear winter, with below freezing temperatures over much of the Northern Hemisphere during summer, occurs because of a reduction of surface solar radiation due to smoke lofted into the stratosphere. WACCM4's more sophisticated aerosol representation removes smoke more quickly, but the magnitude of the climate response is not reduced. In fact, the higher-resolution WACCM4 simulates larger temperature and precipitation reductions than ModelE in the first few years following a 150-Tg soot injection. A strengthening of the northern polar vortex occurs during winter in both simulations in the first year, contributing to above normal, but still below freezing, temperatures in the Arctic and northern Eurasia.

1. Introduction

Since the proliferation of nuclear weapons in the twentieth century, considerable attention has been paid to the impact of a nuclear war on society and the environment. Crutzen and Birks (1982), following previous ideas by Lewis (1979), suggested that massive forest fires ignited by nuclear weapons would rage for weeks after a war, producing a tropospheric pall of smoke that would obscure the Sun and reduce sunlight at the surface for the duration of the fires. Turco et al. (1983) conducted the first climate modeling using a radiative-convective climate model, showing that a *nuclear winter* could occur from this smoke. In a war where nuclear weapons would be used, military and industrial centers located in urban areas would be targeted, which contain fuel loading much higher than forests, thus creating an enormous amount of smoke when burned. Turco et al. (1983) found that urban fires injecting smoke into the upper troposphere could produce severe climate changes and that urban firestorms could inject smoke into the stratosphere, leading to rapid interhemispheric transport and a long-lasting smoke pall, which has since been affirmed by coupled global climate models (Mills et al., 2008; Mills et al., 2014; Pausata et al., 2016; Robock, Oman, & Stenchikov, 2007; Robock, Oman, Stenchikov, Toon, et al., 2007). Aleksandrov and Stenchikov (1983) conducted the first three-dimensional climate modeling for the injection scenarios of Turco et al. (1983) showing that continental temperature reductions would be large despite moderation by the oceans. Malone et al. (1985) conducted the first three-dimensional simulations including smoke transport and removal by precipitation, showing that solar heating could cause smoke in the troposphere to rise into the stratosphere before precipitation removal, greatly prolonging the lifetime of the smoke. The effect of this smoke entering Earth's upper

atmosphere would be to block out sunlight for months to years, decreasing temperatures. In 1986, The Scientific Committee on Problems of the Environment of the International Council of Scientific Unions published a report describing the immense biological, ecological, and human impacts of a nuclear war based on the literature at the time (Pittock et al., 1986). The first simulation with a modern, comprehensive coupled atmosphere-ocean climate model by Robock, Oman, and Stenchikov (2007) showed that solar heating would loft smoke deep into the stratosphere. Robock, Oman, and Stenchikov (2007) confirmed that a nuclear winter would result from the amount of soot that could be produced by a nuclear war between Russia and the United States with current arsenals (Toon et al., 2008). Later agricultural modeling of a regional nuclear war showed an increased likelihood of crop failures and global famine due to the climate effects of smoke (Xia & Robock, 2013; Xia et al., 2015). But climate models have improved since 2007 in terms of horizontal resolution, vertical resolution, and vertical extent, which is essential for an accurate simulation of smoke lofting. We employ the much higher resolution WACCM4 model used by Mills et al. (2014) to repeat the nuclear war scenario from Robock, Oman, and Stenchikov (2007). We incorporate a more sophisticated treatment of stratospheric chemistry compared to Goddard Institute for Space Studies (GISS) ModelE, and aerosol treatment is updated from Mills et al. (2014) by treating the aerosols as fractal particles whose optical properties evolve over time. Only Pausata et al. (2016) has used a model to study the climate effect of nuclear war, using a much smaller injection than here, that allowed for the growth of aerosols in the stratosphere, but their model had a limited vertical resolution and extent (26 levels with a 3-hPa model top), potentially limiting vertical lofting. Mixing together varying ratios of organic and black carbon, Pausata et al. (2016) found a shorter stratospheric residence time of the aerosols due to particle growth. The use of a model with a higher model top and higher vertical resolution here should help to more accurately model the lifetime of fractal smoke particles generated from mass fires, a key uncertainty in this field of study.

A significant climate response is predicated on the basis that vast amounts of smoke would reach the stratosphere, and so an accurate representation of the properties of the aerosols and the amount is crucial. The aerosols produced following the fires ignited by a nuclear explosion would contain organic compounds mixed with elemental carbon, which is also called soot or black carbon. The smoke calculations from Toon et al. (2007) excluded organic carbon, just as most historical climate simulations did, so while including it could increase particle extinction and reduce soot residence time in the stratosphere, as Pausata et al. (2016) found, we exclude it as well. Black carbon is one of the most efficient aerosols at absorbing visible light, allowing for the surrounding air to become buoyant when the aerosols are heated (Ackerman & Toon, 1981; Bond et al., 2013; Turco et al., 1983). For example, a stratospheric injection of a few tenths of a teragram of smoke, containing a few percent of black carbon, from a forest fire in British Columbia in August of 2017 heated the air by about 7 K by absorbing sunlight and lofted the smoke from an injection height of about 12 km to above 20-km altitude within a few weeks (e.g., Khaykin et al., 2018; Peterson et al., 2018; Yu et al., 2019). In contrast, 180 Tg of black carbon (excluding organic compounds that would also be emitted) might be injected in a full scale nuclear war between the United States and Russia from convective plumes from fires (Toon et al., 2008). Self-lofting would allow the aerosols to rise deep into the stratosphere, resulting in a long-duration climate response (Malone et al., 1985, 1986; Robock, Oman, & Stenchikov, 2007, Robock, Oman, Stenchikov, Toon, et al., 2007). Without precipitation to act as a removal mechanism, aerosols would remain in the stratosphere for months to years depending on particle size. Robock, Oman, and Stenchikov (2007) used a model that did not include aerosol particle coagulation and growth and found an *e*-folding lifetime of 4.6 years for soot particles in the stratosphere. However, simulations of massive soot injections of tens of thousands of teragram of black carbon following the impact that killed the dinosaurs showed that particle coagulation should occur, producing large soot particles with greater fall speeds (Bardeen et al., 2017; Toon et al., 2016).

Volcanic eruption clouds provide a well-observed analog for particle lifetimes and climate effects. Sulfate aerosols generated from gases injected into the stratosphere by volcanic eruptions cause global cooling due to the reflection of incoming solar radiation back to space, which has been observed numerous times and modeled successfully (Robock, 2000). Simulations of volcanic clouds including particle growth show that large volcanic eruptions, such as that of Mt. Pinatubo with 35 Tg of sulfate aerosols, produce clouds with lifetimes of about 1 year, as observed (Barnes & Hoffman, 1997; Deshler, 2008). However, numerical simulations suggest that larger eruptions, which are not well observed, will produce large particles with shorter lifetimes (English et al., 2013; Pinto et al., 1989). Volcanic aerosols are not transported as high as black carbon

aerosols as they are only weakly absorptive and do not self-loft significantly (Robock, Oman, & Stenchikov, 2007). Wildfires pale in comparison to the Mt. Pinatubo cloud mass, but their aerosols can heat the air enough to be lofted 8 km vertically (Yu et al., 2019). An injection of 150 Tg of black carbon would be a far greater aerosol loading than wildfire contributions or any volcanic eruptions from the past 100 years (when masses can be reliably determined) but would be orders of magnitude smaller than injections of black carbon into the atmosphere 66 million years ago when an asteroid impact caused much of the biomass on Earth's surface to burn, resulting in a mass extinction event (Bardeen et al., 2017; Toon et al., 2016). Volcanic eruptions and mass fires are both effective methods of injecting aerosols into the stratosphere, but the black carbon produced by nuclear mass fires, like what is simulated here, results in far more extreme climate effects per unit mass.

Cooling at the surface is only one of many phenomena that would occur if abundant black carbon aerosols are injected into the stratosphere. Several modeling studies have shown that stratospheric temperatures would increase by more than 50 K and stratospheric ozone would undergo global destruction, even for a scenario where 5 Tg of soot is injected into the stratosphere (Mills et al., 2014; Robock, Oman, Stenchikov, Toon, et al., 2007; Toon et al., 2007). The global hydrologic cycle would become far less active, with a reduction in summer monsoon precipitation and a significantly reduced growing season (Robock, Oman, & Stenchikov, 2007; Robock, Oman, Stenchikov, Toon, et al., 2007). The impacts on human society would be devastating due to agricultural losses alone, even from the 5-Tg scenario (Xia & Robock, 2013; Xia et al., 2015). Research on the climate impacts of volcanic eruptions has found similar, although usually less severe, consequences as a result of global cooling due to smaller stratospheric aerosol loadings (Robock, 2000).

There are many uncertainties in computing the climate after a nuclear conflict. The greatest uncertainty is how many weapons would be used, what yields would be employed, and which targets would be chosen. This uncertainty cannot be reduced, so ideally, a range of scenarios must be considered to understand the full spectrum of impacts. Using the high-end scenario from Robock, Oman, and Stenchikov (2007), we assume a war between Russia and the United States, involving numbers of weapons allowed under current treaties. The area burned, the amount of fuel available, the amount of smoke and black carbon produced by the fires, as well as the injection altitudes of the smoke, are also uncertain. We use the approach of Toon et al. (2007) who estimated that 180 Tg of black carbon could be emitted into the upper troposphere. Following Robock, Oman, and Stenchikov (2007), we round this estimate downward to 150 Tg, which would double the 20% of black carbon rain-out assumed by Toon et al. (2007) and used by Mills et al. (2008). The soot aerosols are emitted over the continental areas of the United States and Russia following the same idealized approach from Robock, Oman, and Stenchikov (2007). The climate response and smoke removal mechanisms may also differ between models. To date, only Robock, Oman, and Stenchikov (2007) have used a modern climate model to simulate this particular scenario of an all out nuclear war between the United States and Russia. Here we repeat the nuclear war scenario from Robock, Oman, and Stenchikov (2007) using an alternative state-of-the-art modern climate model run at higher resolution and with a more explicit simulation of stratospheric chemistry and aerosols. We then compare our new results to the GISS ModelE simulations from Robock, Oman, and Stenchikov (2007) to help determine how sensitive the climate changes may be to the details of the model and to further constrain the lifetime of black carbon aerosols during this type of black carbon injection.

2. Methods

We use the Community Earth System Model with the Whole Atmosphere Community Climate Model, version 4 (WACCM4) for its atmospheric component. The model has a horizontal resolution of 1.9° × 2.5° (lat-lon), with 66 vertical layers and a model top of 140 km (Marsh, Mills, Kinnison, Lamarque, Calvo, et al., 2013; Bardeen et al., 2017). The Community Land Model 4.0 is used as the land surface model, Parallel Ocean Program v2 is the ocean model, atmospheric CO_2 is set at a constant 370 ppm (levels during the year 2000, same as GISS ModelE), tropospheric aerosols (other than black carbon) are prescribed, and ocean biogeochemistry is included. While full tropospheric chemistry is not included, the transport and removal of soot from fires is handled by the Community Aerosol and Radiation Model for Atmospheres (CARMA). CARMA is a sectional aerosol model, which in this case treats soot as fractal particles

(Bardeen et al., 2008, 2017; Toon et al., 1988; Turco et al., 1979). As a result, the size of particles is not fixed and can change depending on the rate of coagulation and sedimentation. CARMA has 21 different size bins each with different optical properties, such that changing aerosol sizes also changes the amount of extinction and absorption of radiation. This is the same climate model used by Mills et al. (2014), but their simulation kept the particle size of the soot particles fixed at an effective radius of 0.05 μm. Fractal particles using CARMA have a monomer size of 0.03 μm with a fractal dimension varying between 1.5 and 3.0. Hygroscopic growth is not included, but particle coagulation is a function of relative humidity. Despite major improvements in our ability to simulate the evolution of soot particles through time in the stratosphere, photochemical processing and heterogeneous ozone chemistry on the surfaces of the soot aerosols are not represented. The aerosols themselves do not affect the photolysis rates of gas phase chemicals, similar to the models used in Mills et al. (2014) and Pausata et al. (2016). This affects our ability to report on changes in stratospheric ozone, and inclusion of these processes could potentially shorten the residence time of soot particles in the stratosphere.

Robock, Oman, and Stenchikov (2007) reported simulations of a similar war scenario with the GISS ModelE. GISS ModelE is an Earth system model, which was run with a spatial resolution of 4° × 5° (lat-lon), with 23 vertical layers and a model top of 80 km (Schmidt et al., 2006). ModelE included a module to calculate transport and removal of aerosol particles (Koch et al., 2006). At the time, ModelE used a bulk stratospheric aerosol model, without the aerosol microphysics incorporated in WACCM4, where mass extinction and single-scattering albedo were prescribed and sedimentation is a function of particle size. Soot in ModelE was assigned a constant unimodal radius of 0.1 μm, far different from the fractal particles in WACCM4. In ModelE it was assumed that soot could not be removed by rainfall for the first 24 hr, while in WACCM4 soot could immediately be washed out, such that in Mills et al. (2014), 28% of soot was removed before it could be lofted into the stratosphere. Three ModelE ensembles run for 10 years each with no black carbon burden were used as a climatology to compare with the perturbation case, which simulated the 10 years following the injection of soot over the United States and Russia.

As was done in previous model simulations of other nuclear war scenarios (Mills et al., 2008; Mills et al., 2014; Robock, Oman, Stenchikov, Toon, et al., 2007; Stenke et al., 2013), soot is represented as pure black carbon in WACCM4. Extinction per unit mass by soot is computed from the particle size assuming a fractal shape, and a refractive index of 1.8–0.67i, following the approach of Wolf and Toon (2010) and Bardeen et al. (2017). Consequently, the average optical properties vary throughout the simulation as the proportion of black carbon in each bin changes. The mass extinction coefficient for black carbon (for light within the 533-nm centered wavelength band, averaged across all particle sizes) varies between 9.6 and 9.8 m^2/g in WACCM4. In an attempt to account for dust and organic carbon, Robock, Oman, and Stenchikov (2007) reduced the mass extinction coefficient of black carbon to 5.5 m^2/g for all visible light in their 150-Tg case. ModelE also assumed a constant particle size, a constant mass absorption coefficient of 2.0 m^2/g, and a single-scattering albedo of 0.64. However, most nuclear war soot injection estimates and simulations used pure black carbon, assuming that neither dust nor organic carbon would reduce the soot's ability to absorb radiation, while also neglecting their impact on particle size (Bond & Bergstrom, 2006; Toon et al., 2007). In contrast to ModelE, we inject 150 Tg of pure black carbon in WACCM4, where the mass extinction coefficient for particles with an effective radius of 0.1 μm at wavelengths of light at 533 nm is approximately 7 m^2/g. Not using the exact same optical properties of black carbon in WACCM4 as in ModelE sacrifices some direct comparability between the models, but it follows more closely the approach of other model simulations of mass fires as a result of nuclear war. Estimates of smoke emissions by Toon et al. (2008) and others are only for the soot component of the smoke assuming that any organics produced would be oxidized rapidly in the stratosphere. Consideration of composition other than pure black carbon in the smoke would require increasing the mass of smoke emitted in addition to changing the optical properties. Additionally, our model is not yet able to allow the ratio of black and organic carbon in fractal particles to evolve through time, which would be necessary to account for organic carbon properly. Toon et al. (2008) estimated that 180 Tg of black carbon alone could be injected into the atmosphere in the war scenario used here and in ModelE, where urban areas are targeted using 4,400 total nuclear weapons with 100-kt yield from the Russian and United States arsenals (Toon et al., 2008). The United States and Russia each have close to 4,000 strategic weapons deployed or in storage, and the average yield is larger than 100 kt according to recent estimates (Kristensen & Norris, 2018a, 2018b). The approach by Robock, Oman, and Stenchikov (2007)

effectively reduced the total black carbon injected below 150 Tg, which is no longer consistent with estimates of this war scenario (Toon et al., 2007). If Robock, Oman, and Stenchikov (2007) had wanted to consider organic or dust emissions, then the total emissions should have been increased along with changing the optical properties. Here we just consider the black carbon injection of 150 Tg, which is consistent with the emission estimates for this war scenario. We ran three ensembles of WACCM4 for 20 years each with no black carbon burden to use as a climatology to compare with a soot injection case.

The black carbon is injected into the upper troposphere (300–150 hPa) at a rate that is linearly decreasing over a 1-week period starting on 15 May and is spread uniformly over the same areas of Russia and the United States as in ModelE. We retain this simplified approach, while in reality, soot injections would initially be focused only over areas targeted but over days to weeks would likely spread out similar to our initial injection. The year of the injection will be referred to as *Year 0*, which, in agreement with GISS ModelE, is the year 2000. WACCM4 was run for 20 years following this perturbation, and additional ensemble member simulations were not conducted because the magnitude of the forcing is far greater than natural variations on a global scale. Even for a 5-Tg soot injection, the signal dominates over natural variability (Mills et al., 2014). CO_2 was kept constant.

3. Results

3.1. Transport of Soot Across the Globe, Impact on Radiation, and Soot Fallout

The pattern of smoke emitted during the first week is illustrated in Figure 1, which shows the mass mixing ratio of soot at 250 hPa in the WACCM4 simulation. Intense solar heating of the aerosols generates positive buoyancy over large areas, enabling the aerosols to reach the upper levels of the stratosphere, encountering winds that quickly distribute the smoke over the Earth. After a week, soot can be found throughout most of the Northern Hemisphere (NH), and after 2 weeks it drifts into the Southern Hemisphere. Once emitted in WACCM4, the smoke is heated by sunlight and self-lofts to pressures as low as 0.01 hPa (altitude = 80 km), as illustrated in Figure 2a, which shows the soot mass mixing ratio with height averaged over the Earth through time during the WACCM4 simulation. Because WACCM4 simulates changes in the size of soot particles, there is significant particle growth through time, shown in Figure 2b. The particles in WACCM4 grow to more than 10 times the size of the fixed radius of 0.1-μm particles in GISS ModelE, which has consequences for soot lifetime and scattering. The presence of highly absorptive black carbon aerosols in the stratosphere results in considerably enhanced stratospheric temperatures in both WACCM4 and ModelE (see Figures 2c and 2d). WACCM4 has more vertical levels and a higher model top than GISS ModelE, allowing for more accurate handling of upper level thermodynamic and dynamic processes. Although stratospheric heating is stronger in WACCM4 due to a higher mass absorption coefficient, as evidenced by the larger area of 100 K or greater heating in Figure 2c, it persists for a longer period of time in GISS ModelE due to longer aerosol residence time, as shown by the presence of the 30 K or greater anomaly after more than 10 years.

The time evolution of the zonally averaged aerosol optical depth (AOD) anomaly in both WACCM4 and ModelE is illustrated in Figure 3, where GISS ModelE output is from Robock, Oman, and Stenchikov (2007). The WACCM4 model produces optical depths in both the Northern and Southern Hemispheres, which exceed those from ModelE by a factor of up to 2 in the initial few years. The decision to use pure black carbon in WACCM4 contributes partly to this. The second factor is WACCM4's more sophisticated microphysics scheme, which allows particles to form long chains and causes a steady increase in particle effective radius (and scattering) over time. If the mass extinction coefficient in WACCM4 was reduced by 20% across all wavelengths and particle sizes, so that aerosols with a 0.1-μm effective radius had a mass extinction coefficient of 5.5 m^2/g (like in ModelE), growth still would have resulted in a mass extinction coefficient just larger than 7.5 m^2/g for all particles in the 533-nm band in WACCM4. Therefore, even if the soot in WACCM4 began with the exact same size and optical properties as ModelE, the presence of larger fractal-shaped aerosols still would have promoted higher AOD compared to the smaller, unchanging particles assumed in ModelE. A tipping point is reached after Year 2, when the particles in WACCM4 grow too large and begin to fall out more quickly.

The time evolution of the total amount of soot in the atmospheric column, or soot burden, as simulated by WACCM4 and ModelE is illustrated in Figure 4. Additionally, the soot optical depth in the visible band,

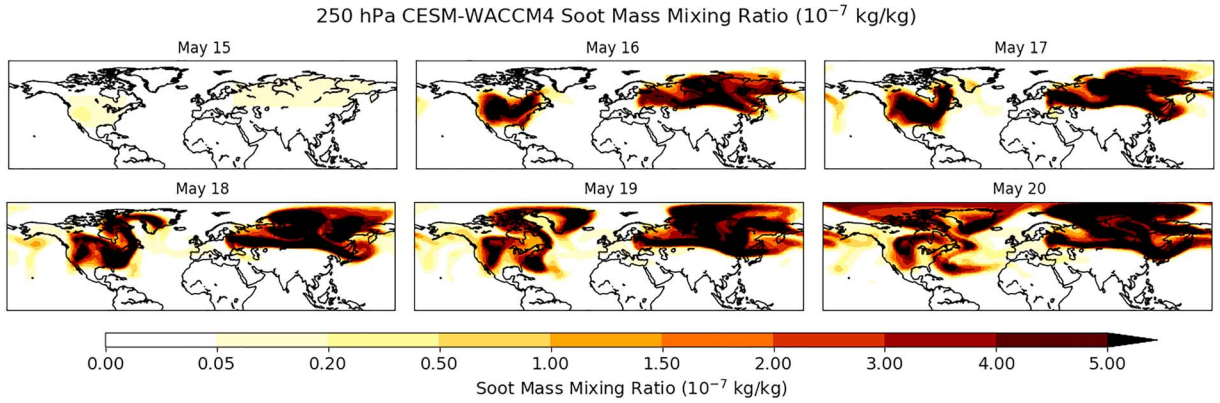

Figure 1. Soot mass mixing ratio (10^{-7} kg/kg) from 15 to 20 May during Year 0, the first 6 days of the 7-day emission period. Emissions are between 300 and 150 hPa over the United States and Russia for 1 week. The soot spreads throughout much of the Northern Hemisphere over this time.

which is calculated at 500 nm in WACCM4, is shown. The initial injection of soot is followed by a gradual decline over the course of a decade. A drop off occurs a few months after the initial injection, but then it levels off during the spring of Year 1. During the next fall, there is another quick drop in total soot burden and a leveling off in the subsequent spring. This *stair-step* pattern continues for the first few years, gradually becoming less prominent as soot is removed at a more constant rate regardless of season after Year 2. Global removal of soot is enhanced during boreal winter in part because the majority of the soot

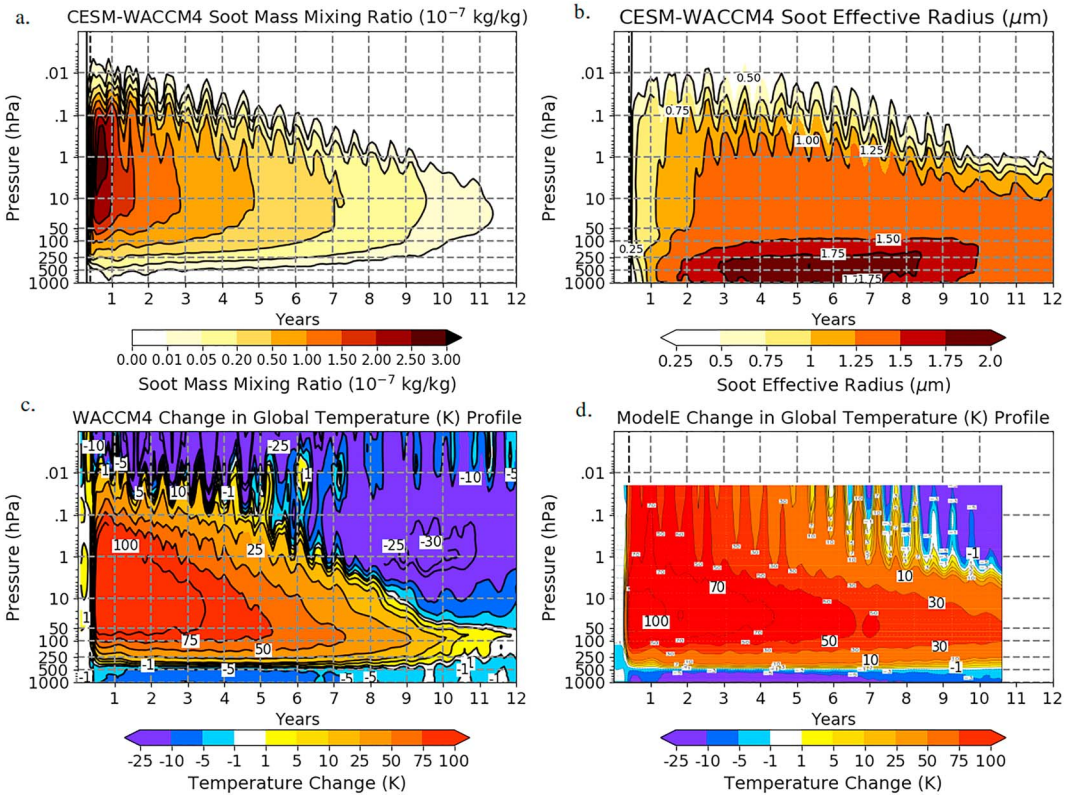

Figure 2. Globally averaged vertical profile of soot mass mixing ratio (10^{-7} kg/kg) after the 150-Tg soot injection on 15 May in Whole Atmosphere Community Climate Model version 4 (WACCM4; top left). Effective radius (μm) of black carbon aerosols during the CESM-WACCM4 150-Tg soot injection simulation (top right). Effective radius of black carbon in Goddard Institute for Space Studies (GISS) ModelE run was a constant 0.1 μm. Temperature profile anomaly following the black carbon injection in WACCM4 (bottom left) and GISS ModelE (bottom right). Extreme heating is observed in the upper troposphere and stratosphere in both models. GISS ModelE figure is from Robock, Oman, and Stenchikov (2007).

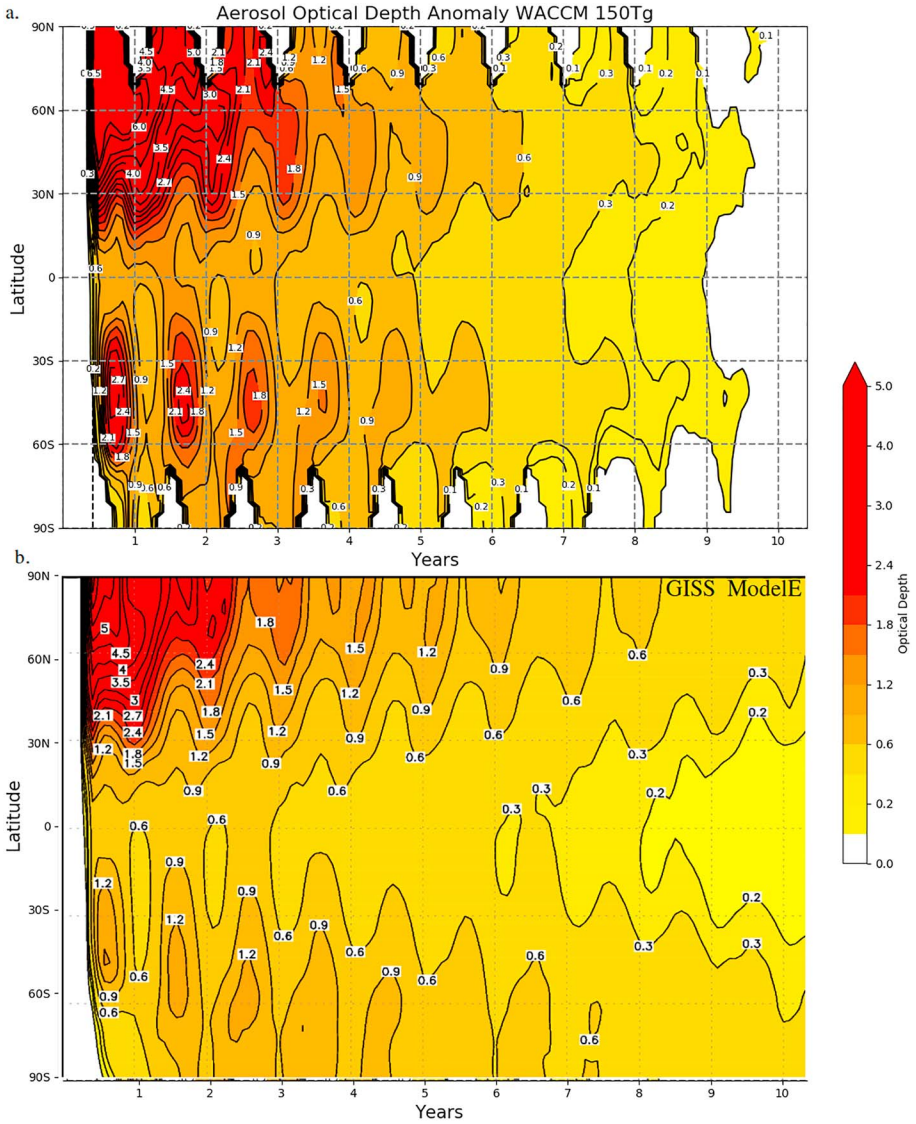

Figure 3. (a) WACCM4 zonal mean visible optical depth anomaly following 150-Tg soot injection into the lower stratosphere. (b) GISS ModelE zonal mean visible optical depth anomaly taken from Robock, Oman, and Stenchikov (2007). Time is measured from 1 January, and the injection occurs from 15 to 22 May.

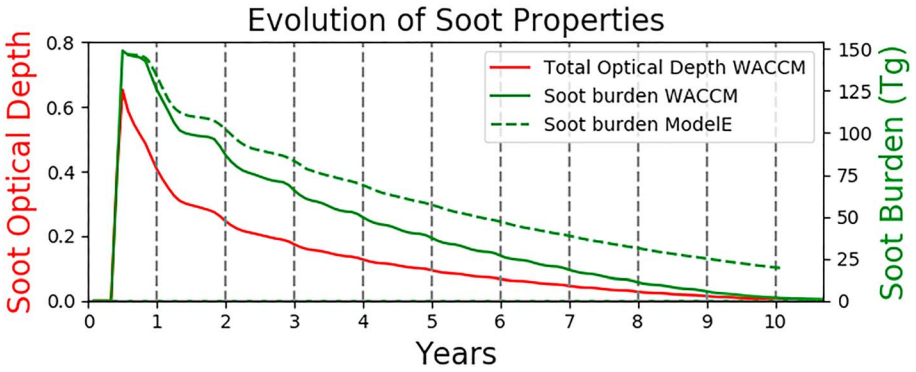

Figure 4. Global soot burden (Tg) and global aerosol optical depth (for visible light) during the WACCM4 simulation. Both variables are through the entire atmospheric column. Output for globally averaged soot optical depth was not saved from Robock, Oman, and Stenchikov (2007).

initially resides in the NH. Soot removal is enhanced especially near the northern polar region during this time mostly due to large-scale descent and reduced heating of aerosols. As the soot becomes evenly spread with time, the effect is reduced. Soot is removed more slowly in ModelE compared to WACCM4, starting with the first winter after the soot injection, and this continues through to the end of the ModelE simulation, where 19 Tg of black carbon is left but less than 2 Tg remains in WACCM4 at the same time.

The mass-weighted global average mass extinction coefficient of black carbon in WACCM4 is 9.6 m^2/g for the first month (at a wavelength of 533 nm) and increases to 9.8 m^2/g during the next few months of the model run, which is its peak value for the simulation. The change in optical depth in WACCM4 closely tracks the change in soot burden, consistent with very little change in the mass extinction coefficient after the first few months. For a wavelength of 533 nm, the mass absorption coefficient is 5.48 m^2/g. Although the size of the aerosols change, the mass absorption coefficient remains constant at 5.48 m^2/g in WACCM4 for particles with an effective radius greater than 0.036 μm (see Figure S1 in the supporting information). After 1 month, nearly 100% of the black carbon aerosols in WACCM4 grow beyond this size. As a result, the aerosols are twice as effective at absorbing shortwave radiation compared to those used in the ModelE experiment. However, variations in the mass extinction coefficient with time are primarily due to changes in scattering as opposed to absorption. The mass extinction coefficient (scattering and absorption combined) as a function of particle radius for a number of wavelengths of light in CARMA is shown in Figure 5. The properties of the particles used in ModelE are also designated in Figure 5. There is a peak in mass extinction coefficient near 10 m^2/g for aerosols with an effective radius between 0.3 and 0.56 μm for a wavelength of 533 nm. During the first few months of the simulation, the majority of black carbon aerosols in WACCM4 are within this size range. As most of the particles grow out of this optical *sweet spot*, they become slightly less effective. However, even when the particles in WACCM4 are at their largest sizes, they are still more effective at scattering and absorbing solar radiation than in the unchanging particles in the ModelE simulation. The growth of particles that occurs in WACCM4 (see Figure 2b) causes the aerosols to fall out more quickly than in ModelE, as the largest stratospheric particles preferentially fall into the troposphere, where they are quickly removed by rainfall and sedimentation. A fractal particle requires more mass to fall out through gravitational settling compared to spherical particles, but the aerosols in WACCM4 quickly surpass a threshold where removal becomes rapid. The growth of aerosols reduces their lifetime and alleviates the long-term climate impact.

The smoke optical properties discussed previously are fed into the climate model's radiation codes. The ModelE and WACCM4 radiative transfer codes are not identical. WACCM4 uses the Rapid Radiative Transfer Model for GCMs code (Iacono et al., 2008; Mlawer et al., 1997), while ModelE's radiative transfer code is as described by Schmidt et al. (2006). Rapid Radiative Transfer Model for GCM uses a two-stream scattering model for solar radiation with 14 shortwave bands and 16 longwave bands. Particles are treated as absorbers of longwave radiation. ModelE has explicit multiple-scattering calculations for shortwave and explicit integrations over both the shortwave and longwave spectral regions. Using a k-distribution approach, 15 noncontiguous shortwave and longwave bands are used to model overlapping cloud, aerosol, and gas absorption (Lacis & Oinas, 1991). Ultimately, we do not expect the differences between the two schemes to play a primary role in differences between climate impacts, but we cannot rule out its effect.

There are many similarities in the initial distribution of the AOD anomaly between WACCM4 and ModelE, shown in Figure 3. Unlike the case of high-latitude volcanic eruptions, whose clouds are generally confined to latitudes poleward of 30° and disappear within less than a year (Robock, 2000), or high-latitude forest fires injecting smoke just above the tropopause, which also seem limited to poleward of 30° (Yu et al., 2019), the emissions from midlatitude urban fires following a nuclear war spread quickly into the Southern Hemisphere. Enhanced lifetime and spread (compared to wildfires and high-latitude volcanic eruptions) occur because the self-lofting of the smoke carries it from the upper troposphere to very high altitudes where it is in the overworld stratosphere, unlike volcanic and forest fire clouds that are injected into the middle world. In the middle world isentropic surfaces connect the midlatitude stratosphere and upper troposphere in the tropics, leading to rapid loss of material into the tropical troposphere (Holton et al., 1995). Once in the stratosphere, soot residence time can also be lengthened by slowing in the Brewer-Dobson circulation due to surface cooling and reduced convection, as was found by Mills et al. (2014).

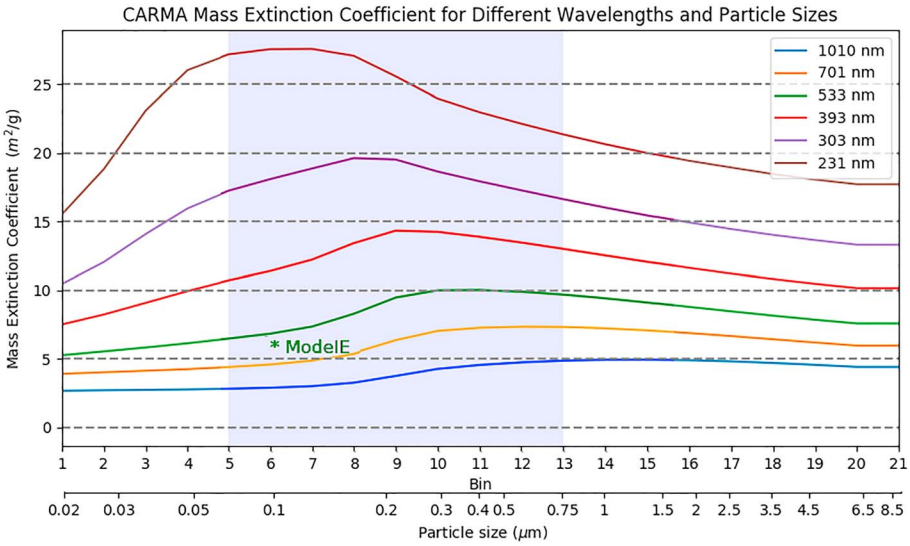

Figure 5. Mass extinction coefficient (m^2/g) for 21 particle sizes (effective radius for fractal particles in WACCM4-CARMA, radius for spherical particles in ModelE) across five wavelengths (centered around the visible light band). ModelE assumed a mass extinction coefficient of 5.5 m^2/g with particles at a constant size of 0.1 μm. The light gray shading represents the size distribution of 95% of the black carbon in WACCM4 on day 1, where the mean effective radius is initially 0.11 μm and the variance is 1.6 μm.

The effect of particle growth and faster fallout in WACCM4 can be seen in Figure 3, where optical depths fall below 0.1 in Year 8 in WACCM4, while ModelE still has optical depths above 0.2 at Year 10. As particle effective radius increases in WACCM4, sedimentation is enhanced, resulting in lower optical depths after 8 years. Based on previous work, the *e*-folding lifetime for stratospheric soot in ModelE was 4.6 years with an effective radius of 0.1 μm (Robock, Oman, & Stenchikov, 2007). Soot has a residence time of days to weeks in the troposphere due to precipitation washing it out, so these times reflect the stratospheric removal rates (Wang et al., 2014). In the case of simulations of a 5-Tg soot injection in ModelE, the mass *e*-folding time after initial rain-out was longer than for the 150-Tg case in ModelE. An 8.4 year *e*-folding time was reported for the Mills et al. (2014) experiment where 5 Tg of soot with a constant radius of 0.1 μm was injected over India and Pakistan using WACCM4, while 6 years was reported by Robock, Oman, and Stenchikov (2007) using ModelE. The longer lifetime in the 5-Tg experiments of Mills et al. (2014) than in Robock, Oman, and Stenchikov (2007), both of which fixed the soot radius at 0.1 μm, may have been due to the higher model top of WACCM4. A higher model top allowed soot to rise further above the tropopause (Figure 2), and the higher vertical resolution combined with a more accurate simulation of vertical motion resulted in the slowdown of the stratospheric residual circulation in Mills et al. (2008), enhancing soot lifetime. Here, in closer agreement with the sensitivity test in ModelE, we found using CARMA, which for the first time allowed the particles to coagulate, an *e*-folding lifetime of 3.5 years for the soot from a 150-Tg injection (as compared to 4.6 years in GISS ModelE). In the current version of WACCM4 the average effective radius of soot particles grows rapidly during the first 2 years to a size greater than 1 μm, reaching a peak of more than 1.3 μm averaged globally (see Figure 2b).

At the latitudes with the highest optical depths, surface shortwave radiation reductions of 100 W/m^2 continue for 7 years in WACCM4, but for only 4–5 years in ModelE (Figure 6). Although soot fallout occurs more quickly in WACCM4, the aerosols are more effective at blocking sunlight until removal becomes significant, which is around Year 7. Greater reductions in zonal mean shortwave radiation are observed over the subtropics and tropical regions in WACCM4 compared to ModelE, and during summer in each hemisphere, WACCM4 lets in more shortwave radiation at higher latitudes than ModelE (Figure 6c). This indicates a tendency for the aerosols to linger in the tropical stratosphere more so in WACCM4 than in ModelE, related to the higher vertical resolution in WACCM4. Globally averaged, as indicated in Figure 7, both models show reductions of up to 100 W/m^2 during the first year, alongside a dramatic decrease in temperature and precipitation. The total downwelling solar radiation at the surface is only 30–40% of normal (where normal is around 160 W/m^2) during the first 6 months of the soot injection across both models.

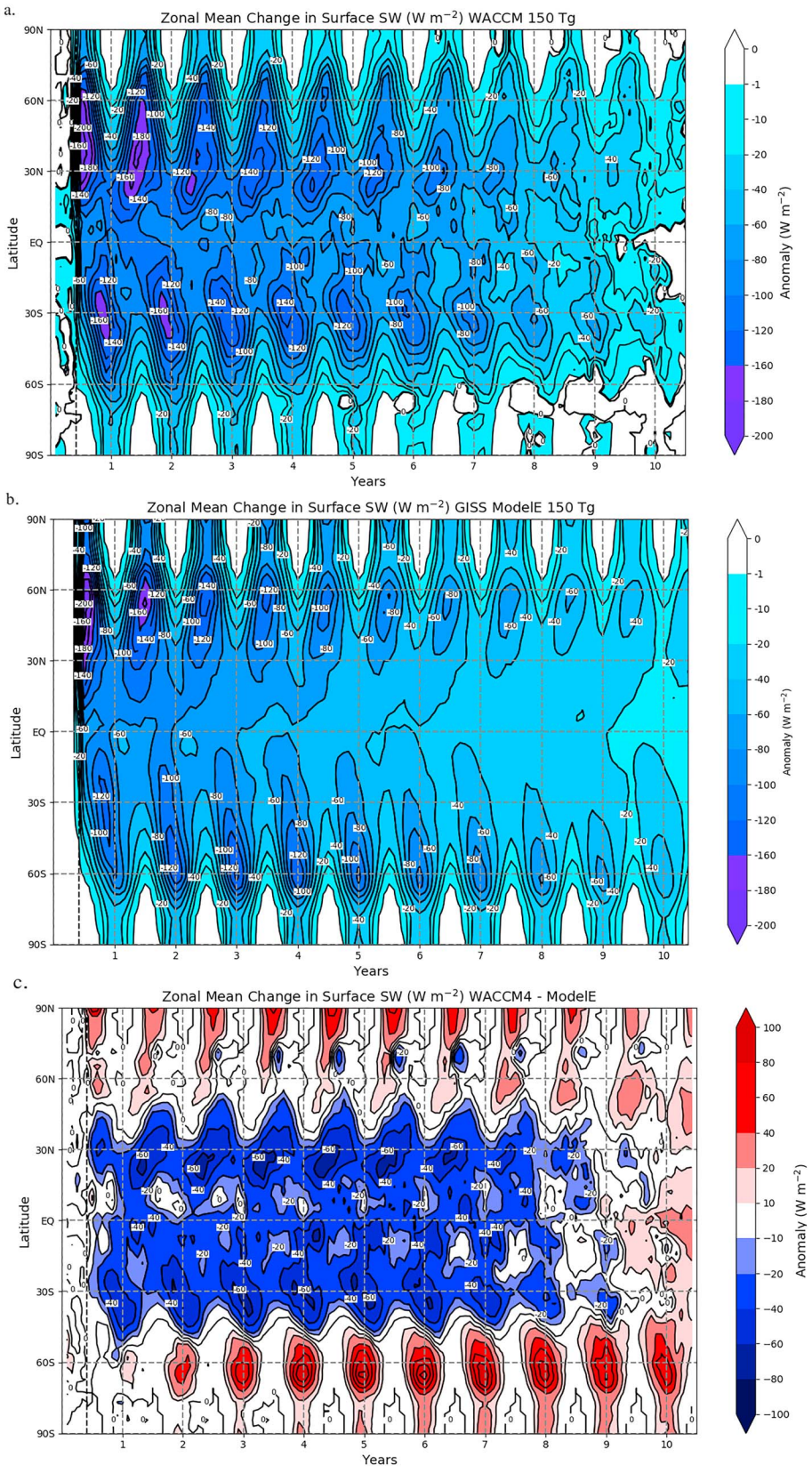

Figure 6. (a) WACCM4 zonal mean surface shortwave radiation anomaly during 150-Tg soot injection from the control run. (b) GISS ModelE zonal mean surface shortwave radiation anomaly. (c) The difference between them.

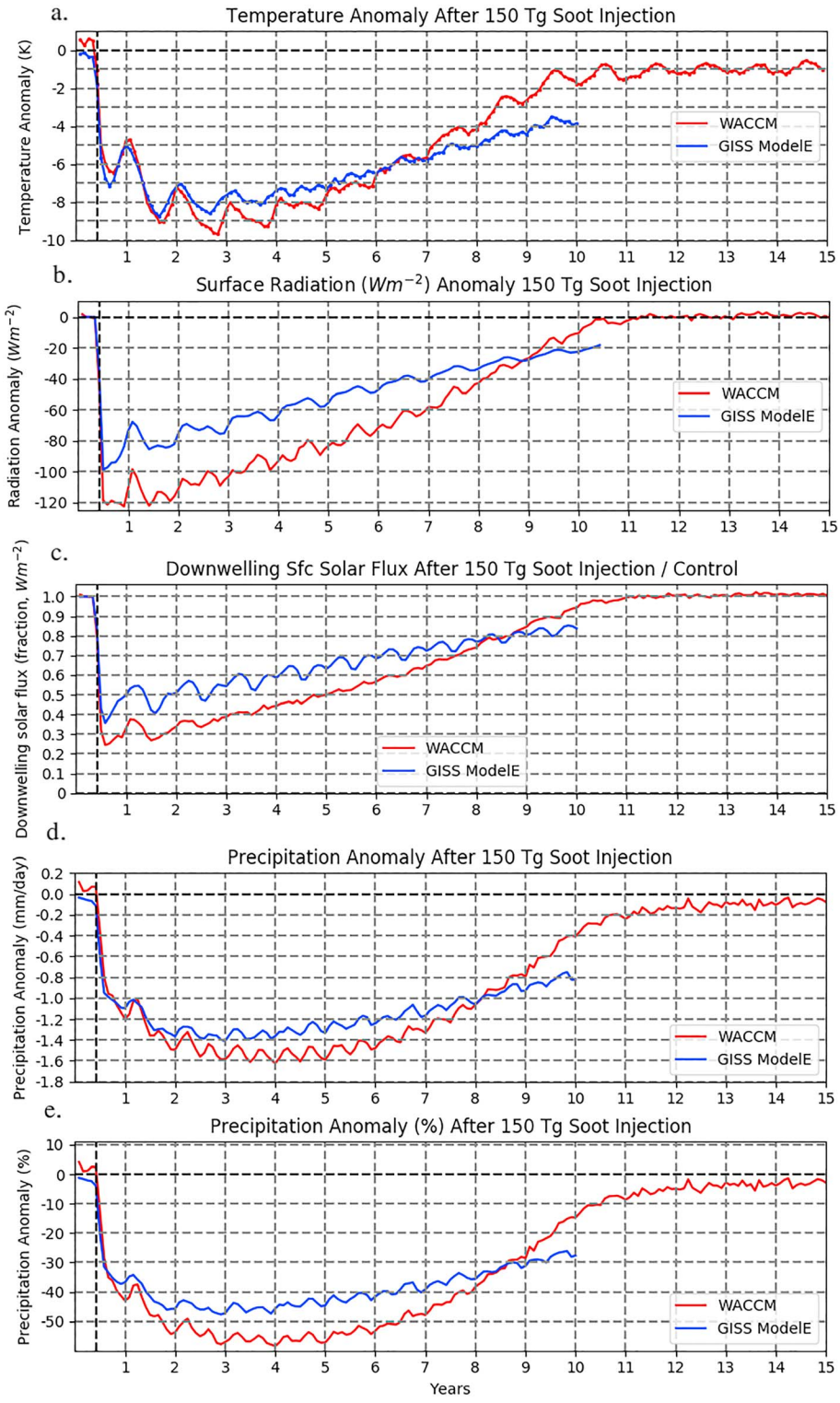

Figure 7. WACCM4 and ModelE monthly global mean (a) surface temperature anomaly (K), (b) surface radiation anomaly (W/m^2), (c) radiation anomaly as a fraction of the control, (d) precipitation anomaly (mm/day), and (e) precipitation anomaly as a fraction of the control following the injection of 150 Tg of black carbon into the upper troposphere and lower stratosphere.

In WACCM4, surface light levels remain below 40% of normal for 3 years, returning to normal after about 10 years after the war starts, while ModelE shows a slower recovery, which is a direct consequence of the small, fixed size aerosols. Low-light levels during the summer months at high latitudes may provide a challenge for organisms that depend on photosynthesis to survive. For example, the base of the photic zone in the ocean, where photosynthesis largely stops, is taken to be at 1% of surface light levels. Bardeen et al. (2017) showed that light levels were well below this limit for the smoke injections that occurred following the impact of the asteroid at the end of the Cretaceous that caused a critical mass extinction event. While parts of the polar latitudes receive less than 5% of normal light during the summer immediately after the 150-Tg soot injection, the K-Pg asteroid extinction event is clearly a far more extreme case.

3.2. Stratospheric Changes: Temperature, Water Vapor, Circulation

Absorption of solar radiation by soot drives extreme stratospheric temperature changes, as mentioned previously and shown in Figure 2. Positive temperature anomalies of more than 100 K occur for about 3 years in the portion of the stratosphere where the bulk of the ozone layer is located in WACCM4. ModelE has slightly less heating for the same time and location, a difference that is consistent with the higher optical depths in WACCM4 as shown in Figure 3 and the higher mass absorption coefficient. As discussed by Mills et al. (2014) and Bardeen et al. (2017), increases in temperature of this magnitude result in dramatic losses of stratospheric ozone, allowing more unfiltered UV radiation to reach the surface. WACCM4 also observed ozone loss, while ModelE did not compute changes in ozone. Heating due to soot occurs down to about 500 hPa, which pushes the tropopause down to very low altitudes, warming the tropopause. Stratospheric water vapor is typically limited by the temperature of the tropopause, so water vapor in the stratosphere increases after the nuclear conflict, as seen in the global profile of specific humidity and relative humidity anomalies after the conflict in Figure 8. Variations in water vapor in the WACCM4 control run are shown in Figure S2, along with actual specific humidity and relative humidity values for the perturbed and control run. Water vapor intrusions, also found by Mills et al. (2014) and Bardeen et al. (2017), are significant for ozone chemistry in the stratosphere, as the photolysis of water vapor exacerbates ozone destruction, which already is increased due to the stratospheric heating (Mills et al., 2014). As black carbon aerosols in WACCM4 stick together and their effective radius grows in size, they become vulnerable to removal from the stratosphere, which may be exacerbated by the intrusion of water vapor. While the lower stratosphere experiences an increase in water vapor (greater than 0.1 g/kg), the local temperature change is so great that the relative humidity is actually reduced by 10–25% for 7 years after the soot injection. Around Year 4, water vapor enters the upper stratosphere (10 to 0.01 hPa) and remains through Year 12. Around Year 9, as the black carbon aerosols are being removed from the lower stratosphere, the temperature of the stratosphere drops, while the water vapor content remains relatively constant, causing a 25–50% increase in relative humidity. A similar phenomenon in the study of the K-Pg asteroid impact by Bardeen et al. (2017) led to the rapid removal of black carbon from the stratosphere, as local regions of the stratosphere become saturated with water and formed clouds that precipitate the black carbon. Although an increase in relative humidity is observed here, the rate of black carbon removal is mostly unchanged during this time (see Figure 4), similar to what was observed by Mills et al. (2014) in a study with a smaller soot injection.

Mills et al. (2014) also observed a slowing of the overturning circulation in the stratosphere, known as the Brewer-Dobson circulation. Surface cooling reduced tropical tropospheric updrafts by 50% in a 5-Tg nuclear war case, and here, using a very similar model with 150 Tg of soot, we observed a reduction in vertical velocity of greater than 80% for up to 4 years. The clear slowing of the overturning circulation of the stratosphere, the layer where most of the aerosols reside, would act to lengthen the residence time of aerosols after they are injected. However, it is apparent that aerosol growth mitigates this effect, as the aerosols fall out more quickly than in ModelE.

3.3. Surface Temperature Change

In both the GISS ModelE and WACCM4 model simulations, global mean surface temperatures drop considerably immediately following the soot injection, as seen in Figure 7. In the first year following the injection, global temperatures plunge by more than 7 K in both models, with some subtle differences. A larger negative shortwave radiation forcing is observed in WACCM4 for 8 years after the injection of soot, and yet, ModelE is 0.5 K cooler during the first summer and follows the WACCM4 temperature response very closely for 18 months after the injection of soot. This indicates that WACCM4 surface temperature is

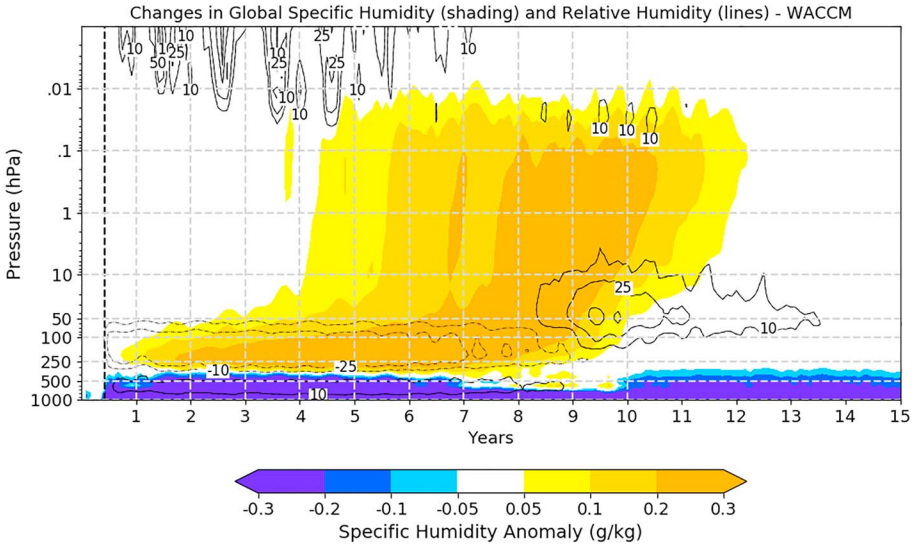

Figure 8. WACCM4 change in global profile of specific humidity (g/kg) and relative humidity (%) following 150-Tg soot injection. Increase in moisture is observed in the lower stratosphere just months after the injection of soot, and increase in the upper stratosphere is observed 4 years following the injection.

less sensitive to a given negative shortwave radiative forcing compared to ModelE. One year after the injection of soot, global temperatures in WACCM4 have declined by 9.5 K from the climatological mean, cooler than ModelE by less than 0.2 K. From the middle of Year 1 through to the beginning of Year 6, WACCM4 remains colder than ModelE, which is also reflected in global precipitation and surface radiation. Figure 7 shows that the negative shortwave forcing reaches its maximum in Year 1, while temperatures continue to decline or remain low through Year 4. It quickly becomes clear that the temperature is not simply tracking the available sunlight, as the high thermal inertia of the oceans delays the minimum global temperature until 2 years after the injection.

Averaged globally, as shown in Figure 7, the WACCM4 simulation is 1 to 2 K colder than ModelE during Years 2 through 5 but by year 6 the WACCM4 and ModelE global temperature anomalies are both −6 K, and WACCM4 is warming up more rapidly. The speed of global temperature recovery in WACCM4 is faster than ModelE starting in Year 5. By Year 7, WACCM4 is warmer than ModelE, despite the stronger negative shortwave radiation forcing in WACCM4. WACCM4 begins to warm up more quickly, while the negative shortwave radiative forcing is still greater in WACCM4 compared to ModelE, but the gap between the two models shrinks for most of the simulation. When the effect of the larger aerosols falling out in WACCM4 is realized in the surface shortwave radiative anomaly near the end of Year 8, WACCM4 is already 1.5 K warmer than ModelE and recovering much more quickly. The quicker return to near zero radiative forcing from black carbon in WACCM4 is due to previously mentioned differences in aerosol treatment, but the response in temperature to a deficit in surface radiation is clearly different between the two models. By Year 10, there is no negative shortwave radiation anomaly in WACCM4. Global mean surface temperatures remain depressed by 0.5 to 1 K below the control climatology for up to 15 years after the soot injection due to the large heat capacity of the oceans and expansion of sea ice across the NH, which prevents it from rapidly warming back to prewar temperatures. ModelE was only run for 10 years, but a prolonged temperature response was also observed in the 5-Tg case using WACCM4 (Mills et al., 2014).

Bardeen et al. (2017) showed that high stratospheric temperatures, similar to those observed here, can greatly increase the downwelling infrared energy at the surface. In our simulation, the globally averaged budget of downwelling longwave radiation at the surface is overwhelmingly negative in response to the cooling of the lower atmosphere. This is contrary to what was found in the K-Pg asteroid impact case with very high aerosol loadings and near total darkness (Bardeen et al., 2017). Significantly more shortwave radiation is able to reach the surface, while more longwave radiates out to space during these nuclear war simulations. However, there is a very small increase in downward longwave radiation at higher latitudes during the winter, which is related to winter warming in this region.

Global surface temperature anomalies vary in space and in time, but similar spatial patterns are observed in both models, as shown in the December-January-February (DJF) Year 0–1 and June-July-August (JJA) Year 1 temperature anomalies in Figure 9. Regardless of season, the largest temperature change is observed over continents. A seasonal bias in the global mean surface temperature, which is obvious from the seasonal cycle from Figure 7, is observed due to the larger fraction of land mass in the NH, which allows larger temperature swings than the ocean. Negative temperature anomalies are strongest in NH summer (JJA) and weakest during NH winter (DJF) for the first 4 years. The difference in the temperature response between DJF and JJA shrinks rapidly in the ModelE simulation after Year 3 as the oceans are responding to the forcing and the forcing itself becomes smaller, reducing the amplitude of the seasonality in the response. Cooling is less significant in the Southern Ocean in both models (see JJA in Figure 9), because the Antarctic polar vortex is strengthened, causing a poleward shift in winds, which reduces the surface westerlies and vertical mixing (Robock, Oman, Stenchikov, Toon, et al., 2007). The presence of absorbing aerosols in the stratosphere alters atmospheric dynamics, similar to the mechanism behind the *winter warming* response observed in the NH following large tropical volcanic eruptions (Groisman, 1992; Robock & Mao, 1992; Stenchikov et al., 2002; Zambri et al., 2017).

Despite such a large aerosol loading, temperatures are warmer than the long-term control mean across the Arctic in both model simulations during the first two winters. While temperatures are warmer, they are still below freezing on average in the Arctic. Figure 9 shows that parts of Scandinavia and areas just north of Eurasia are significantly warmer than normal in both WACCM4 and ModelE during the first full winter following the soot injection. This warming persists to a smaller degree during the second winter as well. Compared to ModelE, the WACCM4 simulation is warmer in the Antarctic and Arctic consistently after Year 1 and cooler in much of the tropics through Year 7. The high-latitude temperature pattern is indicative of the strongly positive Arctic Oscillation in the stratosphere (250 to 10 hPa) that propagates down into the troposphere each winter. As a result, relatively warm air over the Atlantic Ocean is advected northward. This circulation pattern occurs for multiple winters, but its temperature signature is obscured by global cooling after 2 years.

There is a true nuclear winter in both of these simulations, where temperatures drop below freezing over much of the NH during the height of summer. Figure 9 shows temperature anomalies for WACCM4 and ModelE during the second NH summer after the injection (JJA Year 1), one of the coldest summers after the injection. Continental North America and Eurasia are 20 K or more below average for up to three summers after the soot injection. Temperature changes of this magnitude would lead to below freezing summer temperatures for much of the midlatitudes. The red line shown in Figure 9 represents locations, poleward of which the actual temperature is below 0 °C during JJA Year 1, which shows a shift as far south as northern Texas, Arkansas, and Missouri in the United States, imperiling important agricultural areas during that summer.

Temperatures below 0 °C in midsummer cause a near 90% reduction in the growing season in some locations, defined here and in Robock, Oman, and Stenchikov (2007) as the number of consecutive days with minimum temperatures above freezing. Figure 10 shows the length of the growing season (number of consecutive days with minimum nighttime temperatures above 0 °C) in the control run and for Years 1 to 2 in the 150-Tg soot injection run. In the NH, the growing season is measured from 1 January to 31 December and the Southern Hemisphere is from 1 July to 30 June. The length of the growing season drops below 50 days across much of the interior United States and below 100 days for the most agriculturally productive regions in the U.S. Most of Eastern Europe's growing season is reduced below 50 days, and all parts of Russia have their growing season reduced below 25 days. Hard freezes, where temperatures drop below −4 °C, would occur through Years 2 and 3 in the summer, making it impossible to grow crops in the United States and Russia. Ukraine, Poland, and Germany would suffer similar fates, while in China, only the southeast part of the country would stay above freezing during the summer. WACCM4 produces slightly colder temperatures than ModelE, but the temperature in both simulations would be perilous for agriculture.

Robock, Oman, and Stenchikov (2007) examined the impacts of a nuclear winter at a more local level through an analysis of minimum temperatures in Iowa (42°N, 95°W) and Ukraine (50°N, 30°E) using GISS ModelE, showing that a 150-Tg soot injection would produce below freezing temperatures in Iowa throughout the first 2 years after a full-scale nuclear war except for a few days barely above freezing in

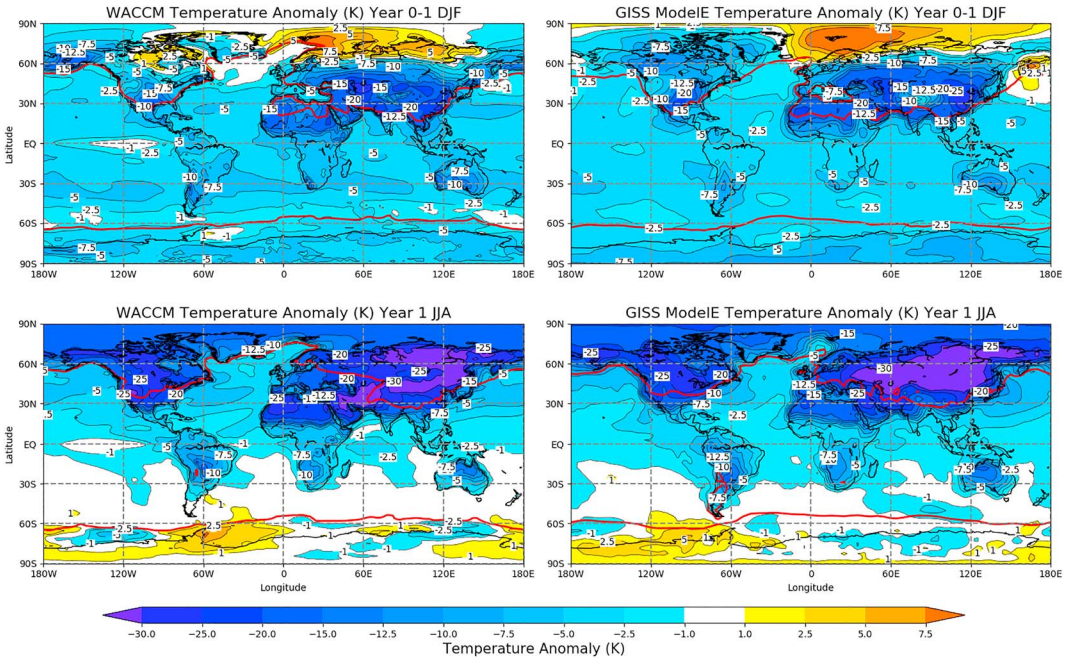

Figure 9. WACCM4 and ModelE temperature anomalies (K) for DJF Year 0–1 (a, b). JJA Year 1 temperature anomalies for WACCM4 (c) and ModelE (d). Anomalies are calculated with respect to the control runs for each model. The red contour represents the latitude, poleward of which, the actual temperature is below 0 °C.

midsummer. In Ukraine, GISS ModelE found below freezing temperatures for two full years, with temperatures barely above freezing in the summer of the second year. The same analysis is performed here and is shown in Figure 11 for WACCM4. Temperatures drop below freezing in Iowa within 1 week following the soot injection on 15 May, and daily minimum temperatures rise above freezing only once in a span of 730 days. Minimum temperatures only consistently rise above freezing during the third summer after the initial injection of soot. In Ukraine, the first summer after the war is not as cold as Iowa, but minimum daily temperatures frequently drop below freezing. During the next summer, Ukraine minimum daily temperatures remain close to freezing but still with days at a time recording below freezing temperatures. This behavior continues through the third summer after the war, when minimum daily temperatures rise to the 5 °C range in both Ukraine and Iowa. Clearly, a nuclear war producing 150 Tg of black carbon would decimate agricultural output at midlatitudes, as even a smaller regional nuclear war led to a reduction in Chinese maize and rice production by 15% for 5 years in an agricultural modeling study (Xia et al., 2015).

3.4. Precipitation Changes

Aerosol-forced reductions in solar heating, evaporation, and convection diminish precipitation globally, which is found in both the WACCM4 and ModelE simulations, as seen in Figure 7 and discussed by Robock, Oman, and Stenchikov (2007). Figure 7 shows the global precipitation response in both models over the course of 10 years, where there is agreement in an immediate, 30% decline in global precipitation through the first few months of the soot injection. Through Years 2–8 the WACCM4 simulation, compared to ModelE, has 10% less (−0.3 mm/day) precipitation. The maximum reduction of globally averaged precipitation in WACCM4 is 58% and in GISS ModelE is 47%, both during the end of Year 3 and beginning of Year 4. During Year 7, globally averaged precipitation increases sharply in the WACCM4 run, while the ModelE simulation recovers very slowly. The rebound in global precipitation lags the global temperature rebound by 1–2 years, but this is a similar pattern to aerosol optical depths between the two models.

Precipitation changes are heterogeneous in space, as some, primarily arid, regions experience increased precipitation despite the extreme global reduction. Figure 12 shows JJA precipitation anomalies for both WACCM4 and ModelE. Averaged globally, WACCM4 has a stronger reduction in precipitation, but there

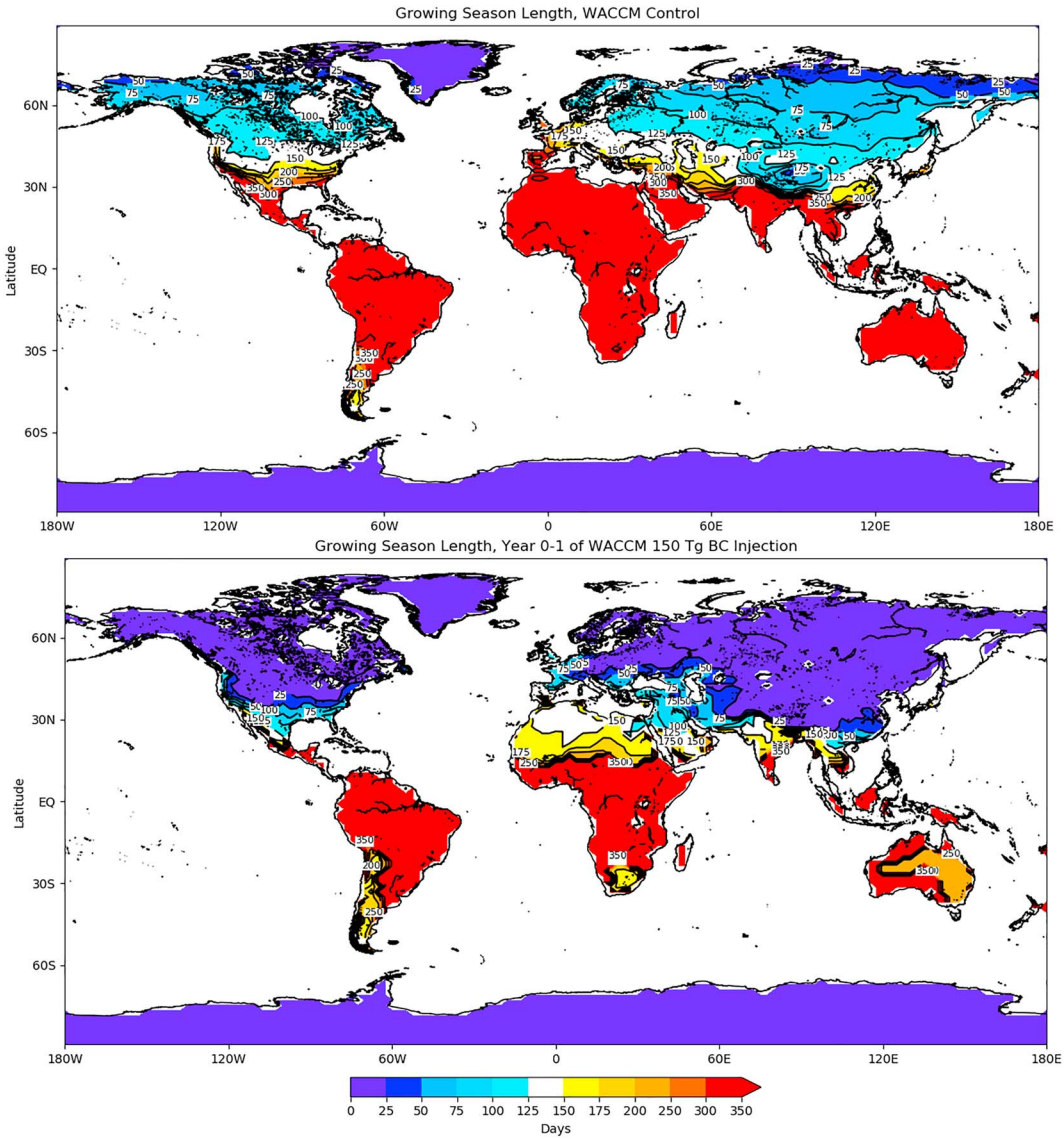

Figure 10. Average growing season length during the WACCM control run (a) and the growing season length during Year 1–2 of the WACCM 150-Tg soot injection (b). For the Northern Hemisphere, this time period corresponds to 1 January, Year 1, to 31 December, Year 1, and in the Southern Hemisphere this corresponds to 1 July, Year 1, to 30 June, Year 2.

are far more extremes in the spatial distribution of precipitation changes. Other than the reductions in precipitation across much of the continental areas in the high latitudes due to reduced evaporation, the most obvious change is the 100% and greater increase in precipitation in the eastern equatorial Pacific Ocean, especially in WACCM4. This pattern resembles the precipitation pattern of a moderate to strong El Niño in the WACCM4 control. The Southern Oscillation Index, the normalized pressure difference between Darwin and Tahiti, undergoes a rapid negative change, resulting in persistent atmospheric El Niño conditions for more than 7 years after the injection of soot. El Niño conditions are common following volcanic eruptions, which have been attributed to mechanisms ranging from land-sea temperature contrasts to southward Intertropical Convergence Zone (ITCZ) shifts to eastward propagating Kelvin waves originating from Africa (Khodri et al., 2017; Pausata et al., 2015; Stevenson et al., 2016). Despite the rapid global cooling, a warm tongue is observed in the sea surface temperatures of the eastern equatorial Pacific from August of Year 0 to February of Year 1. Westerly trade wind anomalies up to and exceeding 14 m/s develop across much of the Pacific Ocean for almost a year, which appear to originate over the Maritime Continent and Southeast Asia. Cold air settles in across the entire eastern portion of the Asian

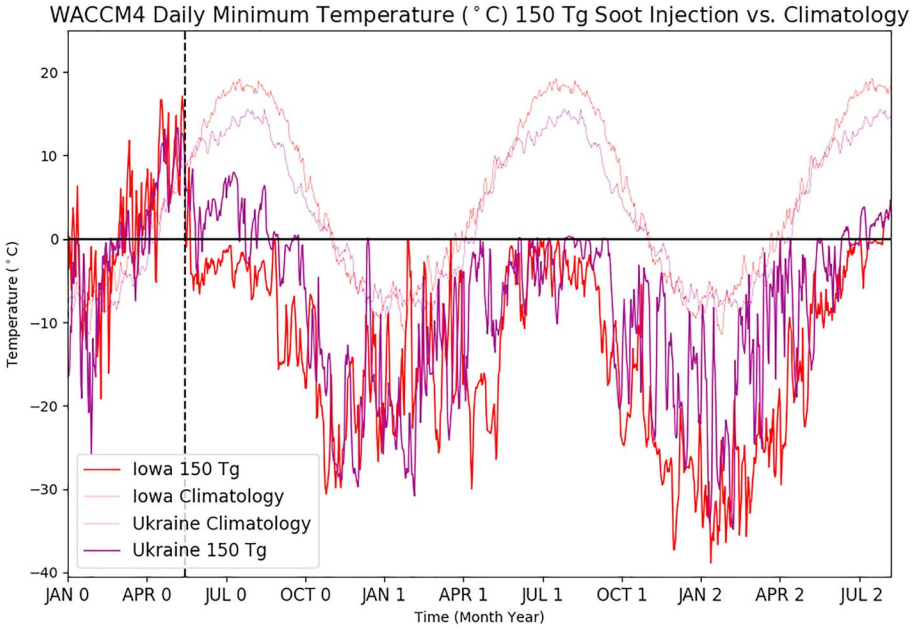

Figure 11. Time series of daily minimum temperature from WACCM4 with 150-Tg soot injection for Iowa (42°N, 95°W) and Ukraine (50°N, 30°E), as well as control run temperatures. The vertical dashed line is the time of soot injection.

continent, causing anomalously high pressure to develop over the continent, producing an intense Asian winter monsoon pattern across the western Pacific for many years, regardless of the season. Intense westerly wind anomalies across the Pacific Ocean result in convection focused over the eastern equatorial Pacific, as well as moderate warming across the region. As a result of this change in circulation coupled with a reduction in evaporation, southern Asia suffers from a collapse of the summer monsoon in WACCM4, which is present in ModelE as well to a lesser degree. The weakening of the summer monsoon has been observed following volcanic eruptions, as continents cool more than the ocean, reducing the land-ocean temperature gradient (Iles & Hegerl, 2014; Trenberth & Dai, 2007; Zambri et al., 2017). In the WACCM4 simulation, the summer Asian monsoon does not return for at least 7 years.

Both WACCM4 and ModelE agree on large precipitation reductions over southern Asia, across the western coast of central Africa, as well as in changes to the position of the ITCZ. The ITCZ, a band of clouds located where the trade winds converge, shifts southward during JJA and northward during DJF and tends to move toward the warmer hemisphere (Broccoli et al., 2006; Donohoe et al., 2012). Greater NH cooling during the summer months leads to a southward shift in the ITCZ. The 6-month average position of the ITCZ, which was typically 3–4°N latitude during the WACCM4 control run, drops as far south as 2.5°S within months of the soot injection. Less solar heating and convection in tropical areas leads to a shift in the Hadley cell, weakening the rising branch (see Figure S3), resulting in a considerable decline in tropical rainfall in the general region of the equator to 20°N in the JJA season. The descending branch of the Hadley circulation is also diminished leading to greater precipitation generally between 20°N and 40°N during JJA, in subtropical deserts such as the Sahara, and desert regions of Australia, South America, and South Africa. In addition to temperature being unsustainable for agriculture, the lack of rainfall in the tropics could affect agriculture.

A 100% precipitation increase (+1 mm/day) over the Arctic Ocean just north of Europe during the first full NH winter after the nuclear war in both model simulations is a result of a dramatic change in the NH wintertime circulation pattern. As mentioned previously, the net energy balance is positive over the Arctic in winter due to advection of warm air from the Atlantic and thermal radiation emitted downward from the hot stratosphere. Overall, the summer monsoons weaken drastically, the average ITCZ location annually shifts southward, and precipitation increases over similar regions in both simulations. Compared to the ModelE, WACCM4 shows a stronger reduction in the Asian monsoon through Year 6, followed by faster recovery as the aerosols fall out.

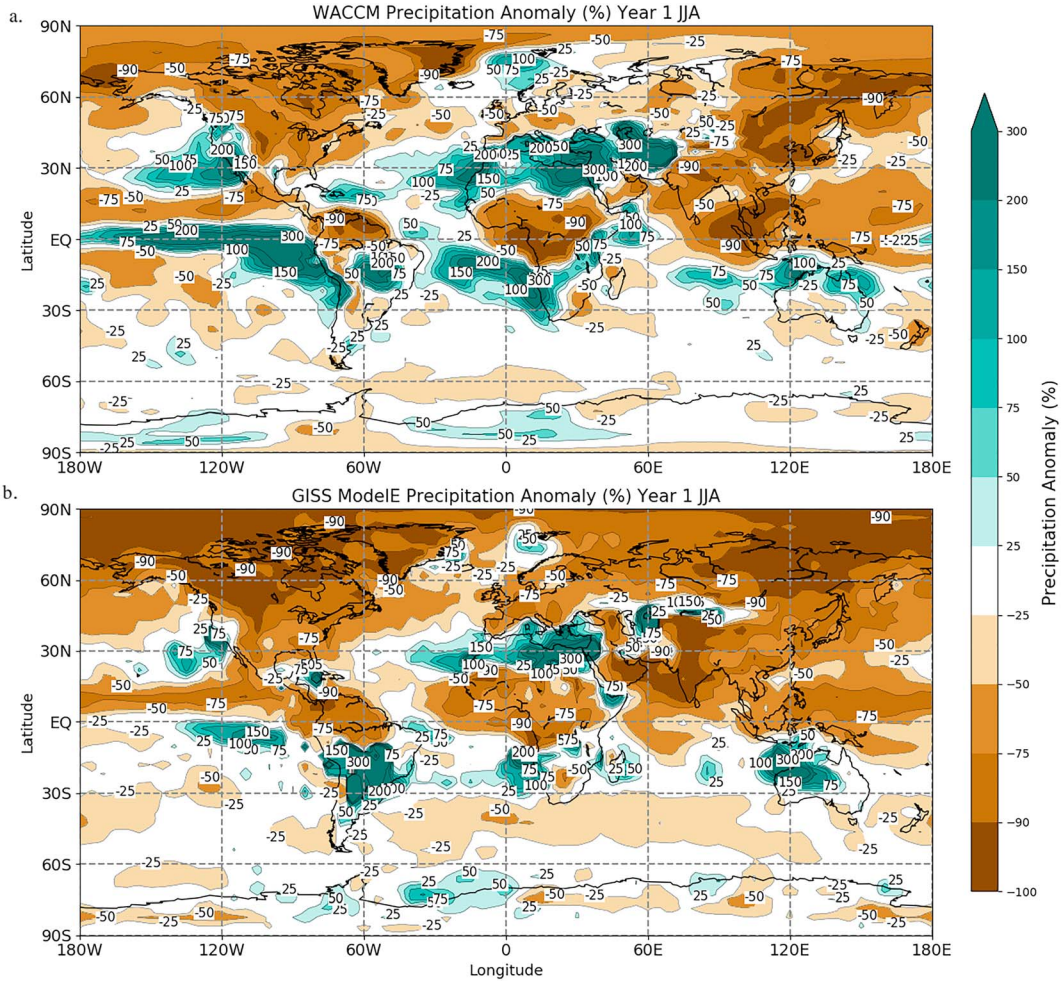

Figure 12. WACCM4 (top) and GISS (bottom) precipitation anomalies (% change) in JJA of Year 1, starting with the second June after the May injection.

3.5. Changes in Circulation

During boreal winter, when no sunlight reaches the northern pole, soot in the midlatitudes continues to absorb sunlight, leading to warming in the midlatitudes and cooling in the polar stratosphere. A differential heating gradient develops in the stratosphere during NH winter, which increases the pole-to-equator temperature gradient, strengthening the stratospheric polar vortex (Mao & Robock, 1998; Robock, Oman, Stenchikov, Toon, et al., 2007; Stenchikov et al., 2002). Zonally averaged wind speeds at 10 hPa and 60°N reach more than 150 m/s each winter during the WACCM4 simulation, 250% more than even the greatest wind speed at this level during the control run. With such strong zonal winds, the vortex remains intact until the final breakdown occurs during late spring when sunlight returns to the pole and the temperature gradient is reversed. WACCM4 and ModelE are in agreement on changes in atmospheric circulation, but WACCM4's higher model top and higher vertical resolution are more adept at representing stratospheric variability, making it a better tool to analyze how changes in the stratosphere result in changes in the troposphere (Charlton-Perez et al., 2013; Shaw et al., 2014).

Geopotential heights at 250 hPa for the first six winters after the injection from WACCM4 in Figure 13a show lower heights in the NH polar region and higher heights elsewhere, corresponding to a strong zonal circulation at this level. This height distribution translates into a highly amplified, positive mode of the Arctic Oscillation (AO) at the surface. The AO is calculated from the first empirical orthogonal function of mean sea level pressure from 20°N to 90°N and is normalized with respect to the WACCM4 control run climatology (Thompson & Wallace, 1998). The pattern from Figure 13a is not dependent on level, as a

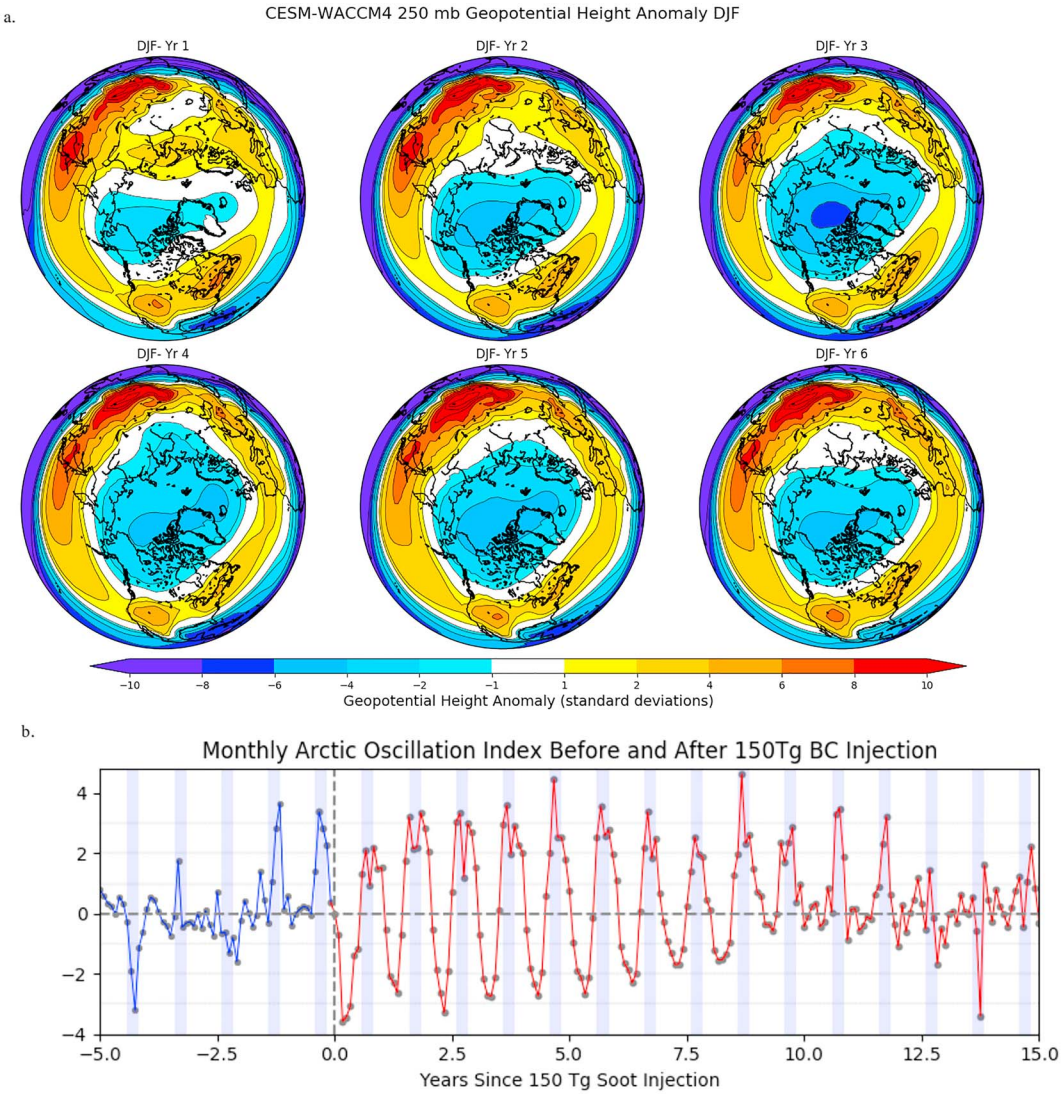

Figure 13. (a) WACCM4 250 hPa geopotential height anomalies (standard deviations from the control mean) for the first six NH winters after the soot injection. (b) WACCM4 monthly Arctic Oscillation (AO) Index during the control run (blue) and after the injection of 150 Tg of soot into the stratosphere (red). DJF is shaded in grey. Positive, amplified AO pattern is observed during DJF, while a negative AO pattern is observed during JJA for the first 9 years.

positive AO response is present from the surface up to 10 hPa (see Figure S4). According to Stenchikov et al. (2002) in a study examining the circulation response to volcanic aerosols following the eruption of Mt. Pinatubo, a tropospheric pathway could also contribute to this pattern, where a reduction in upward propagating planetary waves due to a reduced temperature gradient between the tropics and midlatitudes allows the stratospheric polar vortex to become anomalously strong. The heating in the stratosphere for this scenario is more than 20 times greater than the heating after the Pinatubo eruption. A potential tropospheric pathway's contribution to the positive AO pattern was not examined in detail here because the strength of the stratospheric pole-to-equator temperature gradient is so extreme compared to changes in upward propagating planetary waves. Figure 13b shows the monthly AO index for both the WACCM4 control run and soot injection run. The AO remains amplified and positive (greater than 1.0 averaged over DJF) for 12 consecutive winters after the injection of soot during the WACCM4 simulation. The negative AO present during summer is due to enhanced heating of the aerosols at the pole. The NH winter circulation pattern in ModelE also resembles a positive AO for the 10 years of its run.

The development of a strong stratospheric polar vortex is the main contributor to warming just north of Eurasia, which only stops when the oceanic air upstream cools off after 3 years. The most amplified and

positive AO winters in the WACCM4 control run, when averaged together, produce a temperature signal nearly identical to the observed warming in the first winter after the nuclear winter. The warming in these nuclear winter simulations is slightly north of the expected winter warming following volcanic eruptions and the typical positive AO temperature pattern (Zambri et al., 2017), as a stronger stratospheric pole-to-equator temperature gradient and stronger polar vortex shifts the advection of warm air slightly north. At high latitudes during the winter, an increase in downwelling longwave radiation at the surface is observed, but the spatial pattern, focused over Northern Europe, is more consistent with the change in circulation pattern than the distribution of aerosols. The magnitude of the positive radiative anomaly is within 10% of a composite of all strongly positive winter AO months in the WACCM4 control run, so any contribution from aerosols is minimal. Thus, the positive downwelling longwave radiation anomaly arises from a warmer than normal troposphere, which occurs due to the positive AO circulation pattern.

4. Conclusions

WACCM4, a state-of-the-art climate model, and GISS ModelE, an older climate model, were used more than a decade apart to simulate the environmental aftermath of a full nuclear conflict, a near worst case scenario. The models have significant differences in particle microphysics and spatial resolution, as well as different algorithms for radiative transfer, dynamics, and other modeling approaches. Despite this, the models agree that a nuclear winter would follow a large-scale nuclear war between the United States and Russia, a result previously found by a large number of diverse but much less sophisticated models in the 1980s. Despite differences in sensitivity to shortwave radiative anomalies, both models exhibit a peak temperature drop of near 9 K below climatological values. The massive size of the forcing explains many of the similarities in globally averaged values initially, and differences emerge as the aerosols are removed at different rates. The new model agrees not just in global averages but in spatial patterns for temperature, and precipitation changes and other climate parameters. Both models highlight the risk of a crash in global surface temperatures, but WACCM4 points to a collapse in the summer monsoon, a dramatic shift in El Niño variability, drastic changes to the Northern Hemisphere winter time circulation, and a climate state that is 0.5 to 1 K below climatological temperatures from before the war with no sign of further warming. The WACCM4 model finds that the lifetime of the smoke is greatly enhanced over 1980s models, because it extends to much higher altitudes where the smoke is more isolated from tropospheric rainfall, a result first found in ModelE by Robock, Oman, and Stenchikov (2007).

However, compared to GISS ModelE, the lifetime of soot in the WACCM4 run is shorter due to the inclusion of particle coagulation and fractal optics, despite the higher vertical resolution and model top, alleviating the duration of the most extreme climate effects. Despite this, the cooling for the first few years is more extreme in WACCM4 and temperatures at the end of the simulation suggest a new colder climate state. The inclusion of additional particle removal processes addresses a long-standing uncertainty about the black carbon aerosols released following a nuclear war and allows us to further constrain their *e*-folding lifetime. While we did not consider the effect of organic coatings on top of pure black carbon particles, future work should incorporate more direct calculations of smoke generation using high-resolution fuel loading databases and high-resolution fire modeling of urban landscapes to determine the distribution, type, and amount of material emitted from nuclear fires. Future work will build upon the results of Yu et al. (2019) to quantify the role of organic carbon in smoke from pyroCbs and the sensitivity tests of different ratios of organic carbon and black carbon by Pausata et al. (2016) for a regional nuclear war. Addressing the uncertainty of aerosol composition would further quantify the lifetime of these aerosols and their effects on chemistry in the stratosphere. The research conducted here supports the results of Turco et al. (1983), Sagan (1984), Pittock et al. (1986), Robock, Oman, and Stenchikov (2007), Mills et al. (2008), Robock and Toon (2012), and Mills et al. (2014) that a full-scale nuclear attack would be suicidal for the country that decides to carry out such an attack. The use of nuclear weapons in this manner by the United States and Russia would have disastrous consequences globally. To completely remove the possibility of an environmental catastrophe as a result of a full-scale nuclear war, decision makers must have a full understanding of the grave climatic consequences of nuclear war and act accordingly. Ultimately, the reduction of nuclear arsenals and the eventual disarmament of all nuclear capable parties are needed.

Acknowledgments

This work is supported by a grant from the Open Philanthropy Project. This work utilized the RMACC Summit supercomputer, which is supported by the National Science Foundation (awards ACI-1532235 and ACI-1532236), the University of Colorado Boulder, and Colorado State University. The Summit supercomputer is a joint effort of the University of Colorado Boulder and Colorado State University. WACCM4 model data are available at https://doi.org/10.6084/m9.figshare.7742735.v1, and GISS ModelE data are available at https://doi.org/10.6084/m9.figshare.7742732.v1.

References

Ackerman, T. P., & Toon, O. B. (1981). Absorption of visible radiation in atmospheres containing mixtures of absorbing and nonabsorbing particles. *Applied Optics*, *20*(20), 3661–3668. https://doi.org/10.1364/AO.20.003661

Aleksandrov, V. V., & Stenchikov, G. L. (1983). On the modelling of the climatic consequences of the nuclear war. In *The Proceeding on* Applied Mathematics (21 pp.). Moscow: Computing Centre, USSR Academy of Sciences.

Bardeen, C. G., Garcia, R. R., Toon, O. B., & Conley, A. J. (2017). On transient climate change at the Cretaceous-Paleogene boundary due to atmospheric soot injections. *Proceedings of the National Academy of Sciences of the United States of America*, *114*, E7415–E7424. https://doi.org/10.1073/pnas.1708980114

Bardeen, C. G., Toon, O. B., Jensen, E. J., Marsh, D. R., & Harvey, V. L. (2008). Numerical simulations of the three-dimensional distribution of meteoric dust in the mesosphere and upper stratosphere. *Journal of Geophysical Research*, *113*, D17202. https://doi.org/10.1029/2007JD009515

Barnes, J. E., & Hoffman, D. J. (1997). Lidar measurements of stratospheric aerosol over Mauna Loa Observatory. *Geophysical Research Letters*, *24*(15), 1923–1926. https://doi.org/10.1029/97GL01943

Bond, T. C., & Bergstrom, R. W. (2006). Light Absorption by Carbonaceous Particles: An Investigative Review. *Aerosol Science and Technology*, *40*(1), 27–67. https://doi.org/10.1080/02786820500421521

Bond, T. C., Doherty, S. J., Fahey, D. W., Forster, P. M., Berntsen, T., DeAngelo, B. J., et al. (2013). Bounding the role of black carbon in the climate system: A scientific assessment. *Journal of Geophysical Research: Atmospheres*, *118*, 5380–5552. https://doi.org/10.1002/jgrd.50171

Broccoli, A. J., Dahl, K. A., & Stouffer, R. J. (2006). Response of the ITCZ to Northern Hemisphere cooling. *Geophysical Research Letters*, *33*, L01702. https://doi.org/10.1029/2005GL024546

Charlton-Perez, A. J., Baldwin, M. P., Birner, T., Black, X. R., Butler, A. H., Calvo, N., et al. (2013). On the lack of stratospheric dynamical variability in low-top versions of the CMIP5 models. *Journal of Geophysical Research: Atmospheres*, *118*, 2494–2505. https://doi.org/10.1002/jgrd.50125

Crutzen, P. J., & Birks, J. W. (1982). The atmosphere after a nuclear war: Twilight at noon. *Ambio*, *50*, 114–125. https://doi.org/10.1007/978-3-319-27460-7_5

Deshler, T. (2008). A review of global stratospheric aerosol: Measurements, importance, life cycle, and local stratospheric aerosol. *Atmospheric Research*, *90*, 223–232. https://doi.org/10.1016/j.atmosres.2008.03.016

Donohoe, A., Marshall, J., Ferreira, D., & McGee, D. (2012). The relationship between ITCZ location and cross-equatorial atmospheric heat transport: From the seasonal cycle to the Last Glacial Maximum. *Journal of Climate*, *26*, 3597–3618. https://doi.org/10.1175/JCLI-D-12-00467.1

English, J. M., Toon, O. B., & Mills, M. J. (2013). Microphysical simulations of large volcanic eruptions: Pinatubo and Toba. *Journal of Geophysical Research: Atmospheres*, *118*, 1880–1895. https://doi.org/10.1002/jgrd.50196

Groisman, P. Y. (1992). Possible regional climate consequences of the Pinatubo eruption: An empirical approach. *Geophysical Research Letters*, *19*(15), 1603–1606. https://doi.org/10.1029/92GL01474

Holton, J., Haynes, P., McIntyre, M., Douglass, A., Rood, R., & Pfister, L. (1995). Stratosphere-troposphere exchange. *Reviews of Geophysics*, *33*(4), 403–439. https://doi.org/10.1029/95RG02097

Iacono, M. J., Delamere, J. S., Mlawer, E. J., Shephard, M. W., Clough, S. A., & Collins, W. D. (2008). Radiative forcing by long-lived greenhouse gases: Calculations with the AER radiative transfer models. *Journal of Geophysical Research*, *113*, D13103. https://doi.org/10.1029/2008JD0009944

Iles, C. E., & Hegerl, G. C. (2014). The global precipitation response to volcanic eruptions in the CMIP5 models. *Environmental Research Letters*, *9*, 104012. https://doi.org/10.1088/1748-9326/9/10/104012

Khaykin, S. M., Godin-Beekmann, S., Hauchecorne, A., Pelon, J., Ravetta, F., & Keckhut, P. (2018). Stratospheric smoke with unprecedentedly high backscatter observed by lidars above southern France. *Geophysical Research Letters*, *45*, 1639–1646. https://doi.org/10.1002/2017GL076763

Khodri, M., Izumo, T., Vialard, J., Janicot, S., Cassou, C., Lengaigne, M., et al. (2017). Tropical explosive volcanic eruptions can trigger El Nino by cooling tropical Africa. *Nature Communications*, *8*, 778. https://doi.org/10.1038/s41467-017-00755-6

Koch, D., Schmidt, G. A., & Field, C. V. (2006). Sulfur, sea salt, and radionuclide aerosols in ModelE. *Journal of Geophysical Research*, *111*, D06206. https://doi.org/10.1029/2004JD005550

Kristensen, H. M., & Norris, R. S. (2018a). United States nuclear forces, 2018. *Bulletin of the Atomic Scientists*, *74*, 120–131. https://doi.org/10.1080/00963402.2018.1438219

Kristensen, H. M., & Norris, R. S. (2018b). Russian nuclear forces, 2018. *Bulletin of the Atomic Scientists*, *74*(3), 185–195. https://doi.org/10.1080/00963402.2018.1462912

Lacis, A. A., & Oinas, V. (1991). A description of the correlated k distribution method for modeling nongray gaseous absorption, thermal emission, and multiple scattering in vertically inhomogeneous atmospheres. *Journal of Geophysical Research*, *96*(D5), 9027. https://doi.org/10.1029/90jd01945

Lewis, K. N. (1979). The prompt and delayed effects of nuclear war. *Scientific American*, *241*(1), 35–47. https://doi.org/10.1038/scientificamerican0779-35

Malone, R. C., Auer, L., Glatzmaier, A., Wood, M., & Toon, O. B. (1986). Nuclear winter—Three dimensional simulation including interactive transport, scavenging and solar heating of smoke. *Journal of Geophysical Research*, *91*(D1), 1039–1053. https://doi.org/10.1029/JD091iD01p01039

Malone, R. C., Auer, L., Glatzmaier, G., Wood, M., & Toon, O. B. (1985). Influence of solar heating and precipitation scavenging on the simulated lifetime of post-nuclear war smoke. *Science*, *230*(4723), 317–319. https://doi.org/10.1126/science.230.4723.317

Mao, J., & Robock, A. (1998). Surface air temperature simulations by AMIP general circulation models: Volcanic and ENSO signals and systematic errors. *Journal of Climate*, *11*(7), 1538–1552. https://doi.org/10.1175/1520-0442(1998)011<1538:SATSBA>2.0.CO;2

Marsh, D. R., Mills, M. J., Kinnison, D. E., Lamarque, J., Calvo, J. N., & Polvani, L. M. (2013). Climate change from 1850 to 2005 simulated in CESM1 (WACCM). *Journal of Climate*, *26*, 7372–7391. https://doi.org/10.1175/JCLI-D-12-00558.1

Mills, M. J., Toon, O. B., Lee-Taylor, J., & Robock, A. (2014). Multidecadal global cooling and unprecedented ozone loss following a regional nuclear conflict. *Earth's Future*, *2*, 161–176. https://doi.org/10.1002/2013EF000205

Mills, M. J., Toon, O. B., Turco, R. P., Kinnison, D. E., & Garcia, R. R. (2008). Massive global ozone loss predicted following regional nuclear conflict. *Proceedings of the National Academy of Sciences*, *105*(14), 5307–5312. https://doi.org/10.1073/pnas.0710058105

Mlawer, E. J., Taubman, S. J., Brown, P. D., Iacono, M. J., & Clough, S. A. (1997). Radiative transfer for inhomogeneous atmospheres: RRTM, a validated correlated-k model for the longwave. *Journal of Geophysical Research*, *102*(D14), 16,663–16,682. https://doi.org/10.1029/97jd00237

Pausata, F., Chafik, L., Caballero, R., & Battisti, D. (2015). Impacts of high-latitude volcanic eruptions on ENSO and AMOC. *Proceedings of the National Academy of Sciences of the United States of America*, *112*, 13,784–13,788. https://doi.org/10.1073/pnas.1509153112

Pausata, F. S. R., Lindvall, J., Ekman, A. M. L., & Svensson, G. (2016). Climate effects of a hypothetical regional nuclear war: Sensitivity to emission duration and particle composition. *Earth's Future*, *4*(11), 498–511. https://doi.org/10.1002/2016EF000415

Peterson, D. A., Campbell, J. R., Hyer, E. J., Fromm, M. D., Kablick, G. P., Cossuth, J. H., & DeLand, M. T. (2018). Wildfire-driven thunderstorms cause a volcanic-like stratospheric injection of smoke. *npj Climate and Atmospheric Science*, *1*, 30. https://doi.org/10.1038/s41612-018-0039-3

Pinto, J., Turco, R. P., & Toon, O. B. (1989). Self-limiting physical and chemical effects in volcanic eruption clouds. *Journal of Geophysical Research*, *94*(D8), 11,165–11,174. https://doi.org/10.1029/JD094iD08p11165

Pittock, A. B., Ackerman, T. P., Crutzen, P. J., MacCracken, M. C., Shapiro, C. S., & Turco, R. P. (1986). *Environmental consequences of nuclear war, SCOPE 28*, *Physical and Atmospheric Effects* (Vol. I). New York: John Wiley.

Robock, A. (2000). Volcanic eruptions and climate. *Reviews of Geophysics*, *38*(2), 191–219. https://doi.org/10.1029/1998rg000054

Robock, A., & Mao, J. (1992). Winter warming from large volcanic eruptions. *Geophysical Research Letters*, *19*(24), 2405–2408. https://doi.org.10.1029/92gl02627

Robock, A., Oman, L., & Stenchikov, G. L. (2007). Nuclear winter revisited with a modern climate model and current nuclear arsenals: Still catastrophic consequences. *Journal of Geophysical Research*, *112*, D13107. https://doi.org/10.1029/2006JD008235

Robock, A., Oman, L., Stenchikov, G. L., Toon, O. B., Bardeen, C., & Turco, R. P. (2007). Climatic consequences of regional nuclear conflicts. *Atmospheric Chemistry and Physics*, *7*, 2003–2012. https://doi.org/10.5194/acp-7-2003-2007

Robock, A., & Toon, O. B. (2012). Self-assured destruction: The climate impacts of nuclear war. *Bulletin of the Atomic Scientists*, *68*, 66–74. https://doi.org/10.1177/0096340212459127

Sagan, C. (1984). Nuclear war and climatic catastrophe—Some policy implications. *Foreign Affairs*, *62*(2), 257–292. https://doi.org/10.2307/20041818

Schmidt, G. A., Ruedy, R., Hansen, J. E., Aleinov, I., Bell, N., Bauer, M., et al. (2006). Present-day atmospheric simulations using ModelE: Comparison to in situ, satellite, and reanalysis data. *Journal of Climate*, *19*, 153–192. https://doi.org/10.1175/JCLI3612.1

Shaw, T., Perlwitz, A. J., & Weiner, O. (2014). Troposphere-stratosphere coupling: Links to North Atlantic weather and climate, including their representation in CMIP5 models. *Journal of Geophysical Research: Atmospheres*, *119*, 5864–5880. https://doi.org/10.1002/2013JD021191

Stenchikov, G., Robock, A., Ramaswamy, V., Schwarzkopf, D., Hamilton, K., & Ramachandran, S. (2002). Arctic Oscillation response to the 1991 Mount Pinatubo eruption: Effects of volcanic aerosols and ozone depletion. *Journal of Geophysical Research*, *107*(D24), 4803. https://doi.org/10.1029/2002JD002090

Stenke, A., Hoyle, C. R., Luo, B., Rozanov, E., Gröbner, J., Maag, L., et al. (2013). Climate and chemistry effects of a regional scale nuclear conflict. *Atmospheric Chemistry and Physics*, *13*(19), 9713–9729. https://doi.org/10.5194/acp-13-9713-2013

Stevenson, S., Otto-Bliesner, B., Fasullo, J., & Brady, E. (2016). El Nino-like hydroclimate responses to last millennium volcanic eruptions. *Journal of Climate*, *29*, 2907–2921. https://doi.org/10.1175/JCLI-D-15-0239.1

Thompson, D. W. J., & Wallace, J. M. (1998). The Arctic Oscillation signature in the wintertime geopotential height and temperature fields. *Geophysical Research Letters*, *25*(9), 1297–1300. https://doi.org/10.1029/98GL00950

Toon, O. B., Bardeen, C., & Garcia, R. (2016). Designing global climate and atmospheric chemistry simulations for 1 km and 10 km diameter asteroid impacts using the properties of ejecta from the K-Pg impact. *Atmospheric Physics and Chemistry*, *16*, 13,185–13,212. https://doi.org/10.5194/acp-16-13185-2016

Toon, O. B., Robock, A., & Turco, R. P. (2008). Environmental consequences of nuclear war. *Physics Today*, *61*, 37–42. https://doi.org/10.1063/1.3047679

Toon, O. B., Robock, A., Turco, R. P., Bardeen, C., Oman, L., & Stenchikov, G. L. (2007). Consequences of regional-scale nuclear conflicts. *Science*, *315*, 1224–1225. https://doi.org/10.1126/science.1137747

Toon, O. B., Turco, R. P., Westphal, D., Malone, R., & Liu, M. S. (1988). A multidimensional model for aerosols—Description of computational analogs. *Journal of the Atmospheric Sciences*, *45*(15), 2123–2144. https://doi.org/10.1175/1520-0469(1988)045<2123:AMMFAD>2.0.CO;2

Trenberth, K. E., & Dai, A. (2007). Effects of Mount Pinatubo volcanic eruption on the hydrological cycle as an analog of geoengineering. *Geophysical Research Letters*, *34*, L15702. https://doi.org/10.1029/2007GL030524

Turco, R. P., Hamill, P., Toon, O. B., Whitten, R. C., & Kiang, C. S. (1979). One-dimensional model describing aerosol formation and evolution in the stratosphere: 1. Physical processes and mathematical analogs. *Journal of the Atmospheric Sciences*, *36*(4), 699–717. https://doi.org/10.1175/1520-0469(1979)036<0699:AODMDA>2.0.CO;2

Turco, R. P., Toon, O. B., Ackerman, T. P., Pollack, J. B., & Sagan, C. (1983). Nuclear winter: Global consequences of multiple nuclear explosions. *Science*, *222*(4630), 1283–1292. https://doi.org/10.1126/science.222.4630.1283

Wang, Q., Jacob, D. J., Spackman, R. J., Perring, A. E., Schwarz, J. P., Moteki, N., et al. (2014). Global budget and radiative forcing of black carbon aerosol: Constraints from pole-to-pole (HIPPO) observations across the Pacific. *Journal of Geophysical Research: Atmospheres*, *119*, 195–206. https://doi.org/10.1002/2013JD020824

Wolf, E. T., & Toon, O. B. (2010). Fractal organic hazes provide an ultraviolet shield for early Earth. *Science*, *328*, 1266–1268. https://doi.org/10.1126/science.1183260

Xia, L., & Robock, A. (2013). Impacts of a nuclear war in South Asia on rice production in mainland China. *Climatic Change*, *116*, 357–372. https://doi.org/10.1007/s10584-012-0475-8

Xia, L., Robock, A., Mills, M., Stenke, A., & Helfand, I. (2015). Decadal reduction of Chinese agriculture after a regional nuclear war. *Earth's Future*, *3*, 37–48. https://doi.org/10.1002/2014EF000283

Yu, P., Toon, O. B., Bardeen, C. G., Zhu, Y., Rosenlof, K. H., Portmann, R. W., et al. (2019). Black carbon lofts wildfire smoke high into the stratosphere to form a persistent plume. *Science*. https://doi.org/10.1126/science.aax1748

Zambri, B., LeGrande, A., Robock, A., & Slawinska, J. (2017). Northern Hemisphere winter warming and summer monsoon reduction after volcanic eruptions over the last millennium. *Journal of Geophysical Research: Atmospheres*, *122*, 7971–7989. https://doi.org/10.1002/2017JD026728